Technical Report

TR-99-24

A laboratory scale analysis of groundwater flow and salinity distribution in the Äspö area

Urban Svensson
Computer-aided Fluid Engineering AB

December 1999

Svensk Kärnbränslehantering AB
Swedish Nuclear Fuel
and Waste Management Co
Box 5864
SE-102 40 Stockholm Sweden
Tel 08-459 84 00
+46 8 459 84 00
Fax 08-661 57 19
+46 8 661 57 19

A laboratory scale analysis of groundwater flow and salinity distribution in the Äspö area

Urban Svensson

Computer-aided Fluid Engineering AB

December 1999

This report concerns a study which was conducted for SKB. The conclusions and viewpoints presented in the report are those of the author(s) and do not necessarily coincide with those of the client.

ABSTRACT

The objective of the study is to develop, calibrate and apply a numerical simulation model of the Äspö Hard Rock Laboratory (HRL). An area of 800 x 600 m^2, centred around the HRL, gives the horizontal extent of the model. In the vertical direction the model covers the depth interval from 200 to 560 metres.

The model is based on a mathematical model that includes equations for the Darcy velocities, mass conservation and salinity distribution. Gravitational effects are thus fully accounted for. A site scale groundwater model was used to generate boundary conditions for all boundaries.

Transmissivities of major fracture zones are based on field data. Fractures and fracture zones with a length scale between 5 and 320 metres are accounted for by a novel method that is based on a discrete fracture network. A small background conductivity is added to account for fractures smaller than the grid size, which is 5 metres.

A calibration of the model is carried out, using field data from the Äspö HRL. A satisfactory agreement with field data is obtained.

Main results from the model include vertical and horizontal sections of flow, salinity and hydraulic head distributions for completed tunnel. A sensitivity study, where the properties of the conductivity field are modified, is also carried out.

The general conclusion of the study is that the model developed can simulate the conditions at the Äspö HRL in a realistic manner.

ABSTRACT (Swedish)

Syftet med studien är att utveckla, kalibrera och tillämpa en numerisk simuleringsmodell för Äspölaboratoriet. Den modellerade arean är 800 x 600 m^2 centrerad runt Äspölaboratoriet. Vertikalt täcker modellen djupintervallet 200 till 560 meter.

Modellen baseras på en matematisk modell som innefattar Darcys ekvationer, konservering av massa och en ekvation för salthaltsfördelningen. Gravitationella effekter är inkluderade i dessa ekvationer.

Transmissiviteter för huvudsakliga sprickzoner baseras på data från fältmätningar. Sprickor och sprickzoner med längdskalor från 5 till 320 meter beaktas genom att ett diskret spricknätverk genereras och representeras som ett konduktivitetsfält i modellen. En mindre bakgrundskonduktivitet adderas för att parametrisera sprickor mindre än 5 meter, som är modellens diskretiseringsskala.

Modellen kalibreras mot fältdata från Äspö HRL. Genom optimering av transmissiviteter och konduktiviteter erhålls en god överensstämmelse med fältdata.

Huvudsakliga resultat från modellen är ett antal horisontella och vertikala snitt genom modellvolymen där flöde, salthalt och tryck redovisas. Detta för färdig tunnel, dvs tunnelfrontsläge 3 600 meter.

En känslighetsstudie, där egenskaperna hos konduktivitetsfältet varieras, genomförs också.

Den generella slutsatsen från studien är att den utvecklade modellen simulerar förhållandena runt Äspölaboratoriet på ett realistiskt sätt.

TABLE OF CONTENTS

1 INTRODUCTION

1.1 BACKGROUND

The Äspö Hard Rock Laboratory (HRL) is an underground research facility which forms an important part of the Swedish programme to dispose of spent nuclear fuel in fractured crystalline bedrock. Äspö was chosen because it represents geologically a variety of typical crystalline bedrock environments, both in terms of lithology and hydrostructural properties. The main objectives of the Äspö programme are to: 1) verify pre-investigation methods (i.e. surface and subsurface studies, mostly from boreholes), 2) finalise detailed characterisation methodology for future transfer to site-specific studies of candidate sites, 3) test models for groundwater flow and radionuclide retention (repository scale), 4) demonstrate repository design, construction and handling methods, and 5) test important parts of the repository system with respect to the long-term performance and safety of a deep disposal system for radioactive waste.

A major milestone was reached 1996 with the completion of the pre-investigation and construction phases. The comprehensive research conducted has enabled valuable development and verification of site characterisation methods applied from the ground surface, boreholes and underground excavations. The hydrogeological characterisation of the area has in this context been revised and updated, see Rhén et al. (1997). The updated conceptual models and data have motivated the present study and will form the basis for the numerical simulations to be presented.

In the safety assessment of a deep repository for spent nuclear fuel, it is expected that numerical simulation models will play an important role. The models can provide estimates of the groundwater flow around the repository and transport times, from the repository to the biosphere, for radioactive tracers. One of the problems when setting up such models concerns scales. We need to consider length scales from 10 metres (canister performance) to a regional scale of perhaps 10 km. Most of the models have so far been set up for a site scale, which typically covers a volume of $1 \times 1 \times 1$ km^3. At the boundaries of a model one needs to make assumptions about the pressure and salinity distributions. The model to be presented in this report will derive boundary conditions from a site scale model, see Svensson (1997b). The site scale model employed boundary conditions from a regional model, see Svensson (1997a); a model that covered a volume of 10 x 10 x 3 km^3. We thus have a systematic refinement, and generation of

boundary conditions, from the regional scale to the finest scale resolved in the present laboratory model, which is 1 metre.

1.2 SITE DESCRIPTION

The Äspö Hard Rock Laboratory is located near the Oskarshamn nuclear power plant on the east cost of Sweden, see Figure 1-1. The access tunnel starts on the mainland, continues under the Baltic and reaches the spiral part of the tunnel beneath the island of Äspö. The total length of the tunnel is 3600 metres and it reaches a depth of 450 metres below ground surface. A vertical elevator shaft connects the laboratory to the Äspö Research Village.

Mean precipitation minus evapotranspiration, P-E, has been estimated to be about 200 mm/year for the region, Rhén et al. (1997). For the island of Äspö one can expect that the groundwater recharge (i.e. P-E) is smaller as the distance to the sea is shorter (no storage of water in lakes and ponds during periods of heavy precipitation). A value of 100 mm/year was used in the site scale model.

Around the island of Äspö the Baltic has a salinity of about 0.6%. It is known from boreholes on Äspö that the fresh water lens below Äspö has a thickness of 100 to 200 metres under natural conditions; below this level the salinity increases to reach a value of about 2% at a depth of 800 metres below ground. As the water density increases with salinity we have a density stratified water below the island of Äspö. This is an important feature of the groundwater flow system.

The horizontal extent of the laboratory model to be presented is marked with a red rectangle in Figure 1-1. The depth interval considered is 200 to 560 metres. In Figure 1-1 a blue rectangle marks a volume to be discussed in the calibration of the model.

1.3 OBJECTIVES

The main objective of the study is to develop and establish an adequate model of the groundwater flow and salinity distribution around the Äspö Hard Rock Laboratory (HRL). With "adequate model" it is understood that the model should be well balanced with respect to expected use, available data, scientific basis and computational resources.

In order to meet the main objective of the study it was decided to emphasise the following aspects of the work:

- Consider the large scale groundwater flow by using boundary conditions derived from a site scale groundwater model.

- Employ a recently developed method, see Svensson (1999), to generate more realistic hydraulic conductivity fields.

- Develop a technique for local refinement of the grid in the laboratory model. This may be needed to simulate rock volumes around various experiments in the Äspö HRL.

- Put emphasis on the calibration process.

- Make the presentation of results, in form of figures, diagrams and tables, extensive.

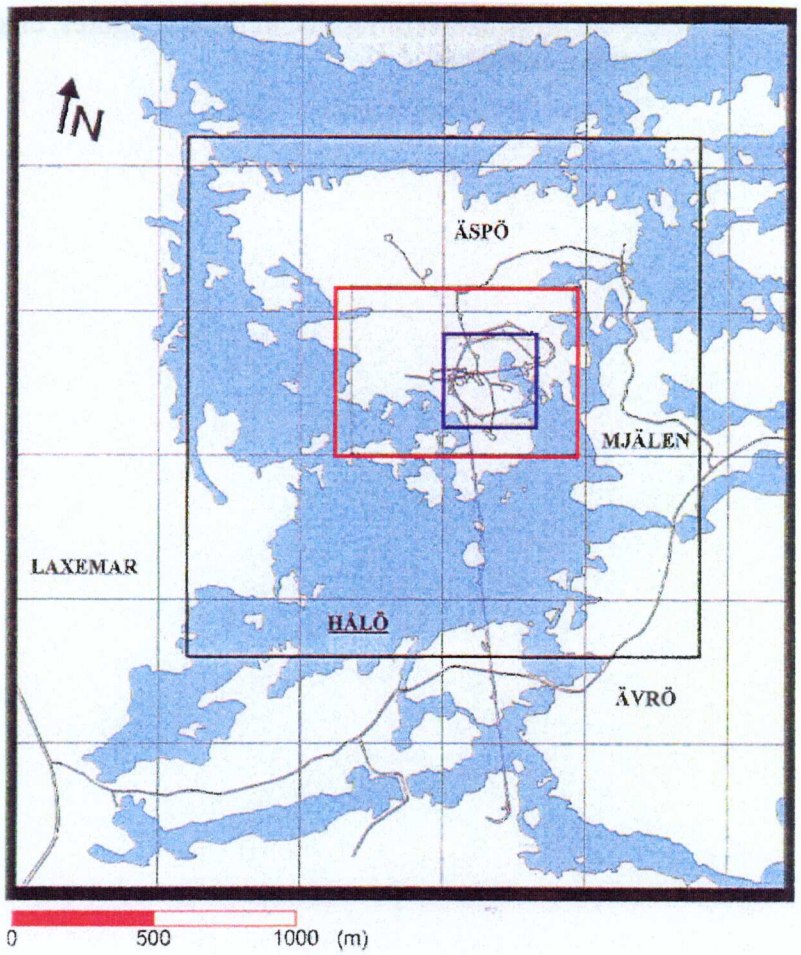

Figure 1-1. *The island of Äspö and the Äspö Hard Rock Laboratory. The black rectangle shows the area of the site scale model, Svensson (1997b). The red rectangle shows the main computational domain considered in this study. The blue rectangle shows an area where a special study of the conductivity statistics on a 3 metres scale will be performed.*

2 BASIC CONCEPTUAL ASSUMPTIONS

2.1 INTRODUCTION

Two main approaches can be identified in the simulations of flow through fractured rocks; the stochastic continuum (SC) technique and the discrete fracture network (DFN) method. The SC-models discretize the computational domain into cells and assign cell conductivities. The DFN-models generate a fracture network, assign transmissivities to each fracture and calculate the flow through the network.

A fundamental problem in the SC-models is to estimate cell conductivities. The usual approach is to base the conductivities on field measurements. Unfortunately, these measurements are often performed at a scale that is smaller than the cell size in the SC-model and it is not clear how to relate the conductivity at one scale to another (upscaling). The fracture network may also include fractures with a scale that is larger than the cell size, which by necessity introduces a correlation in the conductivity between neighbouring cells. A review on available methods to estimate the equivalent conductivity in a heterogeneous medium is given in Renard and Marsily (1997). With equivalent conductivity we will here mean the conductivity that gives the same flow as the heterogeneous media, when the whole computational domain is considered.

In this report an alternative way of estimating cell conductivities in a SC-model will be used. The starting point is the same as for the DFN-model, i.e. a fracture network that is a likely realisation of the fracture system at the site studied. If this fracture network can be correctly represented in a SC-model, it is expected that the resulting conductivity fields will have some desirable properties, like:

- Physical realism. The starting point is a realisation of a fracture network which we expect to represent the hydraulic conductors in the rock volume considered.

- Correlation lengths and anisotropy. If the fracture system is realistic and the representation in the SC-model correct we will get conductivity fields with the correct anisotropy and correlation structure.

As the method has not been used in earlier models of the Äspö site, a brief account of method will be given in this report. A full description of the method, including basic test cases, can be found in Svensson (1999).

2.2 KEY IDEA

Before we discuss how fractures are represented as gridcell conductivities a few characteristics of the computational grid and the fractures need to be introduced. A staggered grid is to be used, which means that scalar quantities, like pressure and salinity, are stored at cell centres while velocity vectors are stored at cell wall centres, see Figure 2-1. Each variable is assumed to be representative for a certain control volume, which is the volume the discretized equations are formulated for. For a velocity cell it is clear that the driving pressure force can be easily formulated. As we are going to apply the Darcy law to the velocity cell we also need a relevant cell conductivity to obtain the cell wall velocity. The conductivity is due to intersecting fractures. In order to describe the effect, we need to define some nomenclature for the fractures, see Figure 2-1. A fracture that has one single opening will in the following be called a single fracture, while a fracture zone consists of several crossing fractures. For a single fracture we call the width of the opening the aperture, which is typically less than 10^{-3} metres. For a major fracture zone the width is typically 10 metres. In the representation as grid cell conductivities we will make no distinction between a single fracture and a fracture zone; both are idealised as a block with dimensions H (height), W (width) and L (length). If the transmissivity of the single fracture, or fracture zone, is denoted T we can define the hydraulic conductivity of the block as $K = T / W$. The key idea of the method can now be stated as follows:

- Fractures and fracture zones are assumed to have a width and a conductivity. They contribute to the conductivity of a velocity cell by an amount which is equal to the intersecting volume times the conductivity of the fracture. Contributions from all fractures and fracture zones that intersect the velocity cell are added and the sum is divided by the cell volume. This gives the conductivity of the velocity cell.

Some illustrations of the concept of intersecting volume can be found in Figure 2-2. For a small fracture the intersecting volume will be the fracture volume, while for a large fracture the cell volume may be the intersecting volume.

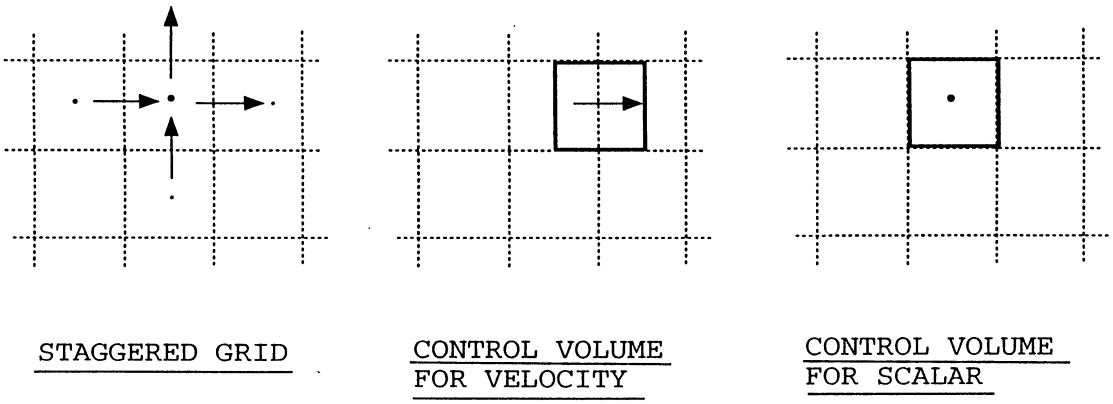

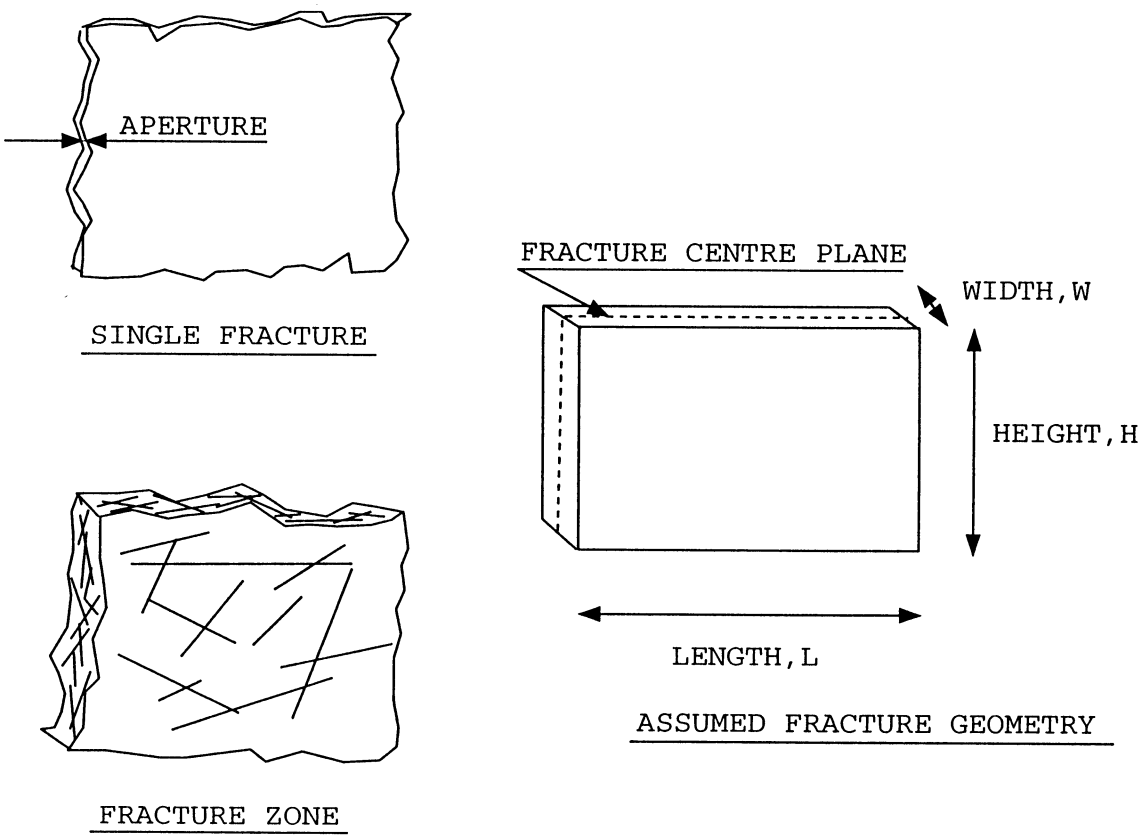

Figure 2-1. *Features of the computational grid (top) and some definitions of the fracture geometry.*

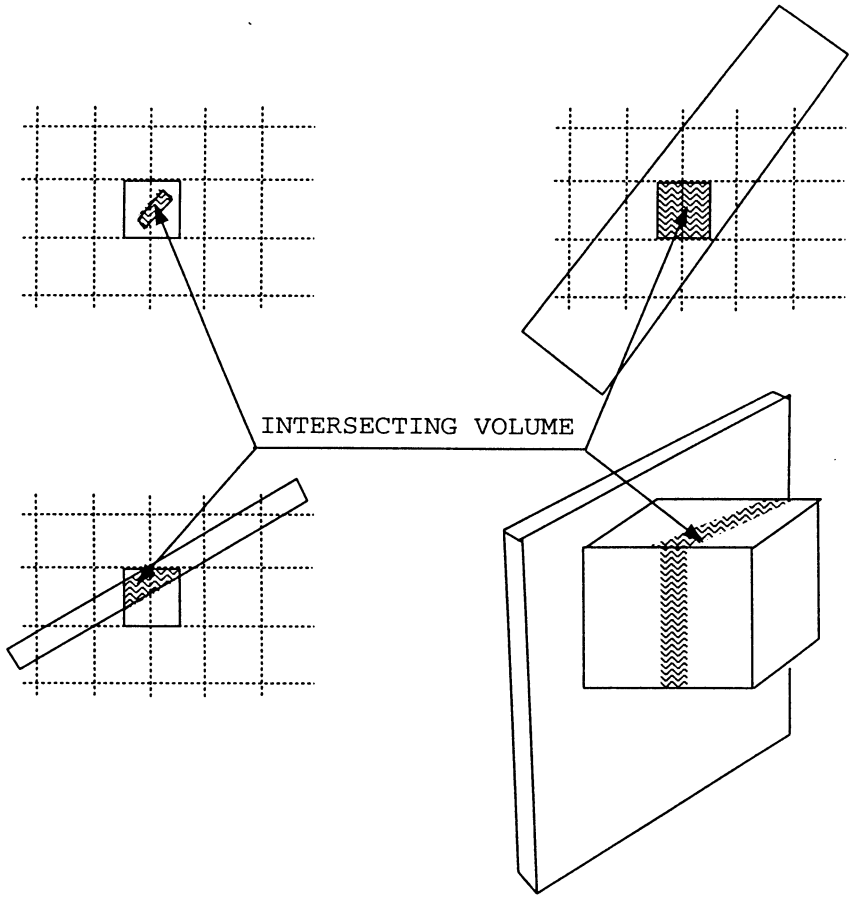

Figure 2-2. *Illustration of the concept of intersecting volume. The shaded areas indicate volumes that intersect a velocity cell.*

2.3 DISCUSSION

The basic principle for calculating cell conductivities is thus quite simple. It remains however to demonstrate that the method is accurate for complex fracture networks. This is the topic of an accompanying report (Svensson, 1999) and will not be discussed in the present context. A general statement about the accuracy of the method will however be given:

- Comparisons with analytical solutions show that the error in the calculated flow through a fracture, or a group of fractures, is less than 2%, provided $W/\Delta > 0.5$, where Δ is the discretisation scale in the computational grid. The error increases somewhat for decreasing W/Δ and it is recommended that $W/\Delta > 0.1$.

From this, and the above mentioned report, one can conclude that the method suggested probably is accurate enough for practical applications. One should note that major fracture zones have a width of 10 to 20 metres and, as Δ will be 5 metres in the present model, $W/\Delta > 1$. The error is then small compared to the uncertainty in transmissivity data. Further details about the accuracy of the method can be found in the above mentioned report.

3 MATHEMATICAL MODEL

3.1 BASIC APPROACH AND REQUIREMENTS

The laboratory model will be used to characterise, in as much detail as possible, the conditions in the rock volume of the Äspö HRL. The main variables of interest are: flow, pressure, salinity and hydraulic conductivity. With this in mind the following basic requirements of the simulation model have been formulated.

- It needs to be three-dimensional with as high resolution in space as possible. Both the fracture network and the various tunnels in the Äspö HRL will be better represented in a grid with high resolution.

- Variable density needs to be accounted for as the salinity of the groundwater will vary in the domain.

The main computational domain was introduced in Figure 1-1. The motives for the size and orientation of the domain can be summarised as follows:

- The orientation should follow the Äspö coordinate system, to facilitate integration with the Äspö data base.

- The computational grid should preferably have a grid spacing of about 5 metres, in order to resolve the fractures and the fracture zones. For the domain indicated in Figure 1-1, this results in a grid of more than 1 000 000 cells.

These considerations led to a domain of 800 x 600 x 360 m^3, centred around the Äspö HRL, represented in a computational grid of 160 x 120 x 72 cells.

3.2 GOVERNING EQUATIONS

For the momentum balance it will be assumed that the Darcy law applies. For the salinity equation we will assume a balance between advective transport and dispersion, i.e. only steady state conditions are to be simulated. For the domain considered it can be expected that the strong forcing of the tunnel, i.e. the inflows, ensures more or less steady state conditions.

Within these assumptions, and the requirements listed in the previous section, the following set of equations can be formulated.

Momentum:

$$0 = -\frac{\partial p}{\partial x} - \frac{\rho g}{K_x} u \tag{1}$$

$$0 = -\frac{\partial p}{\partial y} - \frac{\rho g}{K_y} v \tag{2}$$

$$0 = -\frac{\partial p}{\partial z} - \frac{\rho g}{K_z} w - \rho g \tag{3}$$

Salinity balance:

$$\frac{\partial}{\partial x} us + \frac{\partial}{\partial y} vs + \frac{\partial}{\partial z} ws = \frac{\partial}{\partial x}\left(Dn \frac{\partial s}{\partial x} \right) + \frac{\partial}{\partial y}\left(Dn \frac{\partial s}{\partial y} \right) + \frac{\partial}{\partial z}\left(Dn \frac{\partial s}{\partial z} \right) \tag{4}$$

Mass balance:

$$\frac{\partial}{\partial x} \rho u + \frac{\partial}{\partial y} \rho v + \frac{\partial}{\partial z} \rho w = 0 \tag{5}$$

Equation of state:

$$\rho = \rho_0 (1 + \alpha s) \tag{6}$$

Where u, v, w are Darcy velocities, p pressure, s salinity (in %, by weight), K_x, K_y, K_z conductivities, D hydraulic dispersion coefficient, n kinematic porosity, α a coefficient $\left(= 7.8 \times 10^{-3}\right)$, ρ_0 a reference density of water (= 1 000 kg/m^3), ρ density of water and g gravitational acceleration. The coordinate system is denoted x, y, z with x in the east direction, y north and z vertical upwards.

It is still unclear (at least to the author) how the hydraulic dispersion coefficient ought to be interpreted and determined in a fractured rock. For a general porous media, where a representative elementary volume can be defined, general tensor expressions are available, see Bear and Verruijt (1987). A further complicating factor is that we are going to apply the salinity equation in a discretized form, i.e. on our computational grid. A suggestion is that the dispersion coefficient should account for sub-grid mixing processes. Due to the uncertainty about the interpretation of the process we will assume that the dispersion coefficient is isotropic and proportional to the local velocity and the grid-size, hence:

$$D = \beta\Delta|\vec{U}| \tag{7}$$

where β is an unknown coefficient, Δ the grid-spacing and $|\vec{U}|$ the magnitude of the pore-velocity. As seen, the effect of molecular diffusion is also neglected in (7). As D is multiplied with n in equation (4) we will further assume that $n|\vec{U}|$ is equal to the magnitude of the Darcy velocity. A constant value of 0.5 metre was set for the product $\beta\Delta$.

3.3 GEOMETRIC FRAMEWORK AND MATERIAL PROPERTIES

The major transmissive fracture zones in the region are shown in Figure 3-1. The transmissivities have been estimated by Rhén et al. (1997) and later somewhat modified in a calibration presented in Svensson (1997b). In Table 3-1 the transmissivities of the fracture zones considered in the present computational domains, see Figure 1-1, are given. The calibrated values will be used in this study. Also the widths of the fracture zones (from Rhén et al., 1997) are given in Table 3-1. In the following we will call these major fracture zones the deterministic fracture zones in contrast to the background, or stochastic, fracture network to be described next.

The background fracture network needs to be specified with respect to orientation, size distribution, fracture intensity, width and transmissivity distributions. Here we will choose to leave the transmissivity as a calibration parameter and specify the rest of the properties. Other choices are of course possible, but the transmissivity distribution was chosen as we do not have any field data on this distribution, but we can formulate a calibration criterion related to it (details below). In the present context we will therefore only state that the transmissivity, T, will be related to the fracture size, l:

$$T = f(l) \tag{8}$$

Other properties of the background fracture network are specified as follows:

Fracture orientation. Several projects have been carried out with the objective to characterise the fracture orientation at Äspö. Of special significance for this study are: the TRUE Block Scale Volume (Hermansson et al., 1997), the ZEDEX tunnel (Hermansson et al., 1998) and the TBM tunnel (LaPointe et al., 1995). These rock volumes are part of the present domain and we therefore seek a

consensus based on the above mentioned reports. The following is suggested:

> Three major fracture sets can be identified; one horizontal, one NW trending and one NE trending. The two last ones are subvertical. The horizontal fracture set is believed to be less water conducting. The NW trending set is more conductive, or of higher intensity, than the NE trending set.

From this it is concluded that the fracture network can be based on two vertical fracture sets; one NE trending and one NW trending. Furthermore, in the above mentioned reports the spread around these main orientations was given in form of a Fisher dispersion coefficient, κ. Also in this study we will use a Fisher distribution for the realisation of the network. As the NW-direction should be more conductive, 70% of the fractures will have this trend (with Fisher's $\kappa = 12$) and 30% will have a NE trend (with $\kappa = 7$).

Fracture intensity. The fracture intensity is specified from a power law distribution. For a length interval, *dl*, we then get:

$$n = \mathrm{I} * \left[\left(\frac{l + dl}{l_{ref}} \right)^{\alpha} - \left(\frac{l}{l_{ref}} \right)^{\alpha} \right] / \alpha \qquad (9)$$

where n is the number of fractures per unit volume, I the intensity, l_{ref} a reference length (=500 m) and α, the power law exponent, put to -2.6 (see LaPointe et al., 1999). The intensity was determined to 10^{-8} by generating fractures in the interval 320 to 1 000 metres and compare the number with the number of deterministic fracture zones in the domain. The intensity chosen gives 10 to 15 (different realisations) fracture zones in the length interval which can be compared to 12 deterministic fracture zones.

Fracture shape: The fractures are assumed to be squares, with length, L, and have a constant width, W. In Rhén at al. (1997) major fracture zones are said to have a width larger than 5 metres. The width of the deterministic fracture zones are given in Table 3.1 and, as can be seen, all fracture zones have $W \geq 10$ metres. If we consider the typical length of a deterministic fracture zone to be 500 metres we find that the typical width is $0.02L$. In lack of other information we will use this relation also for the background fracture network, with the restriction that $W / \Delta > 0.1$ (see Section 2.3). It should be noted that the fracture width is not a crucial parameter; it is the transmissivity that largely controls the flow capacity.

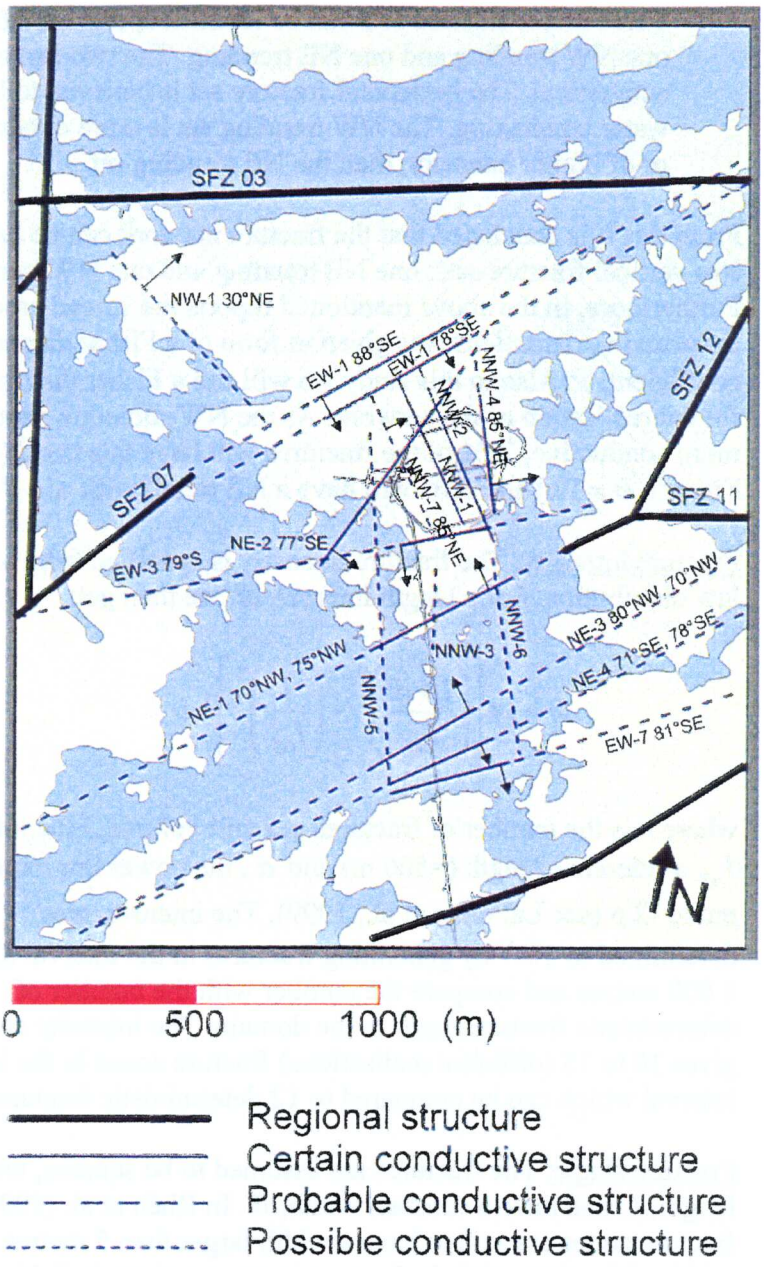

Figure 3-1. *Major fracture zones in the area, after Rhén et al. (1997).*

From this information the background fracture network specified in Table 3-2 can be formulated. As seen, fractures from 5 to 320 metres are generated. The lower limit was chosen to be the same as the grid resolution as only fractures larger than the grid size can contribute to the anisotropy and correlation in the conductivity field. The upper limit is chosen with respect to the deterministic fracture zones, which are typically larger than 300 metres. If fractures smaller than 5 metres should prove to be important, these can be accounted for by adding a background conductivity.

Table 3-1. Transmissivity and width of conductive structures on Äspö, after Rhén et al. (1997).

Fracture zone	Transmissivity x 10^{-5} [m^2/s]		Width [m]
	From Rhén et al. (1997)	Modification due to calibration in Svensson (1997b)	
EW1, 88°	0.052		20
EW1, 78°	1.2		20
EW3	1.7	1.2	10
NE2	0.012	0.8	10
NE1	22.0	30.0	10
NNW1	0.86	3.0	10
NNW2	2.4	1.0	10
NNW3	2.0		10
NNW4	6.5		10
NNW5	0.4		10
NNW6	1.4		10
NNW7	0.75	8.0	10

Table 3-2. The background fracture network.

Fracture set number	Length interval [m]	Numbers generated (one realisation)	Arithmetic mean length [m]	Specified width [m]
1	160-320	33	208	4.2
2	80-160	110	104	2.1
3	40-80	537	52	1.0
4	20-40	2830	26	0.5
5	10-20	15554	13	0.5
6	5-10	92076	6	0.5

3.4 SPATIAL ASSIGNMENT METHOD

All fractures (deterministic and background) will be represented in the computational grid by the method described in Section 2. However, before the fractures are represented as grid conductivities one needs to consider how isolated fractures are to be treated. Depending on the situation studied (to be further discussed in the calibration and result section) we may choose to remove or keep isolated fractures, or groups of fractures, in the conductivity field. If we choose to remove the isolated fractures the following steps are performed:

- The deterministic fractures are considered to be water-conducting and can thus form a "starting" network in the sorting procedure.
- Fractures that cross the boundaries of the domain are not removed as we can not for certain say that these are isolated.
- A sorting procedure determines if a fracture, or a group of fractures, is isolated and, if so, removes these fractures.

3.5 BOUNDARY CONDITIONS

For the cases considered in this report the boundary condition are given as prescribed pressure and salinity. These are generated from the site scale model. Since the gridsize in the site scale model is 20 metres and 5 metres in the laboratory model, linear interpolation was used to generate the intermediate values.

When the Äspö HRL is included in a simulation we need to consider the inflows to the tunnel. These inflows are not boundary conditions in the usual meaning; a more relevant name is perhaps "distribution mass sinks". The measured inflow to tunnel sections need to be assigned to computational cells with a deterministic fracture zone crossing. Based on the measured data given by Rhén et al. (1997), the distributions found in Table 3-3 have been estimated. Distributions are given for the two tunnel front positions to be considered in this report.

An alternative way to describe the influence of the tunnel is to apply a fixed pressure, i.e. atmospheric pressure, in the "tunnel cells". Normally a larger inflow than the measured one will then result and it will be necessary to reduce the conductivity of the cells facing the tunnel. The strength of this extra friction, or skin-resistance, can be determined in an iterative manner from the measured inflow to a certain tunnel section. This method will be tested for the tunnel section 3 100 to 3 600 metres.

3.6 NUMERICAL TOOL AND OUTPUT PARAMETERS

The system of equations is solved by the general equation solver PHOENICS, Spalding (1981). PHOENICS is based on a finite-volume formulation of the basic equations and embodies a wide range of coordinate systems (cartesian, body-fitted, cylindrical, etc) and numerical techniques (higher order schemes, solvers, etc). Output parameters from the code are pressure, salinity and Darcy velocities. It is however simple to generate additional output parameters like hydraulic head and density.

Table 3-3. Inflows to the Äspö HRL. Measured inflows at two tunnel front positions and assigned fracture zones for withdrawal. Basic data from Rhén et al. (1997).

Tunnel section (m)	Measured inflow l/s		Selected zone(s) for withdrawal
	Tunnel front 2875 (m)	Tunnel front 3600 (m)	
1460-1584	0.61	0.61	NE2
1584-1745	0.34	0.27	NNW7
1745-1883	0.52	0.36	NNW1, NNW2
1883-2028	0.63	0.47	NNW4
2028-2178	0.92	0.70	NNW4
2178-2357	1.15	1.42	NNW1, NNW2
2357-2496	0.07	0.17	NE2
2496-2699	0.93	0.93	NNW7
2699-2875	0.59	0.38	NNW1, NNW2
2875-2994		1.12	NNW4
2994-3179		2.33	NNW4
3179-3426		0.96	Atm. Pressure in tunnel
3426-3600		0.46	Atm. Pressure in tunnel
Shaft	3.05	1.54	NNW7

4 CALIBRATION

4.1 INTRODUCTION

A groundwater model is normally calibrated by adjusting conductivities and transmissivities to meet some predefined conditions or criteria, for example the drawdown due to a pump test. This will also be the basic approach in the calibration of the laboratory model. However, it should perhaps be pointed out that the present task is a little bit beyond what is normally included in a calibration process, i.e. adjusting parameters. For the background fracture network we do not know the transmissivity distribution at all and the task is to find a suitable distribution. One may question if this should be called calibration, but the task is anyway included in this section.

As mentioned above, the boundary conditions are generated from the site scale model. For consistency, also the tunnel inflow distribution is taken from the site scale model. The transmissivities of the major fracture zones were calibrated in the site scale model and will not be the subject of calibration here. These conditions and assumptions will strongly determine the flow, pressure and salinity distributions in the laboratory model. It is thus clear that the calibration process is strongly constrained and in practice limited to the influence of the background fracture network.

The objective of the calibration is to generate as realistic conductivity fields as possible for the Äspö HRL. It should be noted that it is a site specific calibration and we therefore make extensive use of data from Äspö HRL.

4.2 CALIBRATION CRITERIA

The following calibration criteria were formulated:

- In a recent study, see Rhén and Forsmark (1998), the frequency of "High Permeability Features" (HPF) was studied. It was concluded that fracture zones with a transmissivity $\geq 10^{-5}$ m^2/s are found with an arithmetic mean distance of 75-105 metres. This includes also the deterministic fracture zones which were found to contribute with about 48% to the total number of fractures found. The arithmetic mean distance between fractures with $T \geq 10^{-6}$ m^2/s was found to be in the range

35-55 metres. We will evaluate the mean arithmetic distances for fractures with $T \geq 10^{-6}$ and $T \geq 10^{-5}$ m^2/s, in the fracture network generated.

- During the construction of the Äspö HRL, the pressure was monitored in a number of borehole sections. The drawdowns at tunnel front position 2875 metres can be found in Rhén et al. (1997); these data will be compared with simulated drawdowns.

- The conductivity distribution for a test-scale of 3 metres has been extensively studied at Äspö, Rhén et al. (1997). The corresponding distribution of cell-conductivities, with $\Delta = 3\,m$, will be calculated and compared with field data.

- We will compare the conductivity fields used in the site-model with the corresponding fields in the laboratory model. For the laboratory model domain we want to ensure that the equivalent conductivity in all three coordinate directions is the same for the two conductivity fields.

Other criteria could have been formulated, but it is believed that the above criteria will constrain the background fracture network in a useful manner. Main arguments for the criteria are:

- The frequency of HPF:s will determine the transmissivity of large background fractures.

- It is essential that the laboratory model predicts the correct pressure drops in the borehole sections in the domain, as we are going to use the model to "describe conditions in experimental volumes".

- By studying the conductivity distribution on the 3 metre scale, we can focus on the distribution of low conductivity cells. This may be essential for transport simulations.

- The comparison with the equivalent conductivity for the site scale model is essential for consistency between the two models. If we have similar equivalent conductivities for the two models we also have the same flux, as we use pressure boundary conditions.

4.3 CALIBRATION PROCESS

The difficult step in the calibration process is to find a strategy for how the calibration criteria should be met. The more linked the criteria are the more difficult the task is. Fortunately, the criteria

above are not strongly linked and the strong influence of boundary conditions and inflows to the tunnel also make the task easier.
A few trial calculations indicated that the following strategy would work:

- First determine the transmissivity distribution for the background fractures.

- The conductivity distribution on a 3 metres scale requires the addition of a background conductivity. The added conductivity is however of the order 10^{-10} m/s and will not strongly influence the other criteria. We can thus perform this operation independently.

- The pressure drops in borehole sections and the equivalent conductivities are to a large extent determined by the deterministic fracture zones, which are not subject to calibration. We thus expect these values to be of the right magnitude independently of other adjustments.

4.4 RESULTS

The main outcome of the calibration is a formula for the transmissivity of the background fractures:

$$T = \begin{cases} 10^{-5}(l/100)^2 & [\mathrm{m}^2/\mathrm{s}] \quad \text{for } l \le 100 \text{ metres} \\ 10^{-5} & [\mathrm{m}^2/\mathrm{s}] \quad \text{for } l > 100 \text{ metres} \end{cases} \qquad (4\text{-}1)$$

The frequency of High Permability Features (HPF) was the most important criterion when establishing this relation, of course it also ensured that the other criteria were fulfilled as well.
Some features, which were considered to be adequate, of this relation include: the maximum transmissivity is of the same order as that for deterministic zones and the transmissivity for $l = 5$ metres is 2.5×10^{-8} m^2/s, which ought to ensure that the smallest fractures do not make a significant contribution to the conductivity field.

As mentioned, the test on a 3 metres scale required the addition of a small background conductivity. It was found that a lognormally distributed conductivity, with $mean(\log_{10}(K)) = -10.0$ and $std.\ dev(\log_{10}(K)) = 0.8$, gives good agreement with field data.

Results will now be presented, which demonstrate that the calibration criteria have been adequately fulfilled.

High Permeability Features. In Figure 4-1 illustrations of conductivity fields based on fractures with $T \geq 10^{-5}$ m^2/s and $T \geq 10^{-6}$ m^2/s are found. The arithmetic mean distances were calculated by drawing a number of lines in the east-west direction and count the number of crossings. It was found that the mean distance for $T \geq 10^{-5}$ m^2/s (which includes deterministic zones) is about 80 metres and that the distance decreases to 57 metres if all fractures with $T \geq 10^{-6}$ m^2/s are counted. The corresponding values from the field measurements are 75-105 metres and 35-55 metres, respectivly.

Drawdowns. The calculated drawdowns in borehole sections in the domain were compared with measured ones, based on a tunnelfront position of 2875 metres. It was anticipated that the drawdowns should be sensitive to various realisations of the background fractures. In order to study this eight realisations of the background fractures were generated and the drawdown for each borehole section and each realisation was calculated. The result can be studied in Table 4-1, the location of boreholes can be found in Figure 4-2. It is seen that different realisations are best for different boreholes. Recognising this pattern, it is tempting to try to optimise the comparison by using what can be called the "Method of local realisation". We thus enclose a borehole in a volume and use fractures from the best realisation in this volume. The fracture centre is used to determine if a fracture belongs to the enclosing volume. This means that a large fracture with its centre outside the volume may still dominate the volume, which shows that there is no guarantee that the method improves the comparison in every borehole.

In Table 4-1 results including local realisations can be found. When using this method one has to decide which realisation should be used outside the volumes enclosing the boreholes. This realisation is called the base realisation in Table 4-1. It is found that the locally optimised fields improve the agreement with measured drawdowns. Some further aspects of the technique will be given in the discussion section and some figures illustrating the "enclosing volumes" will be found later in this section

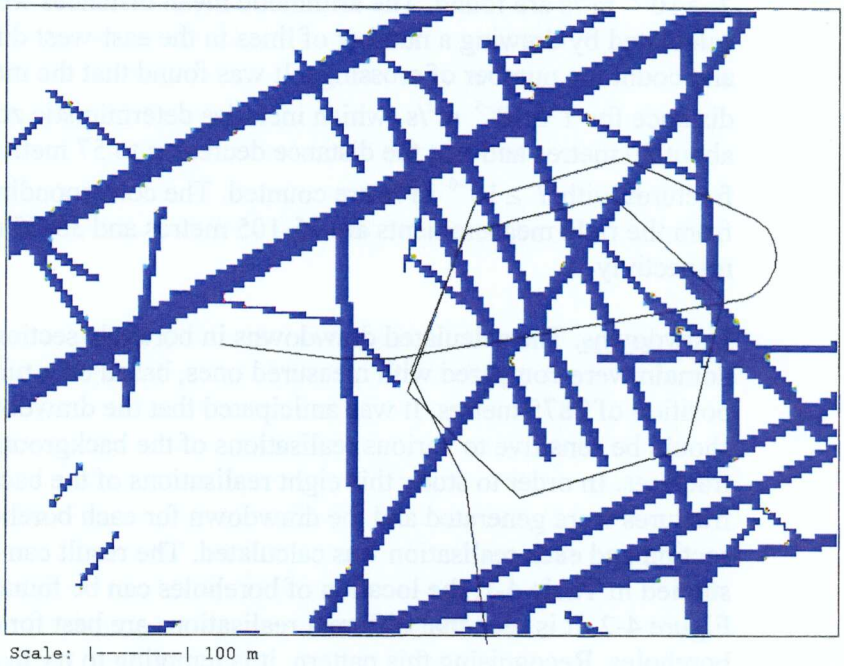

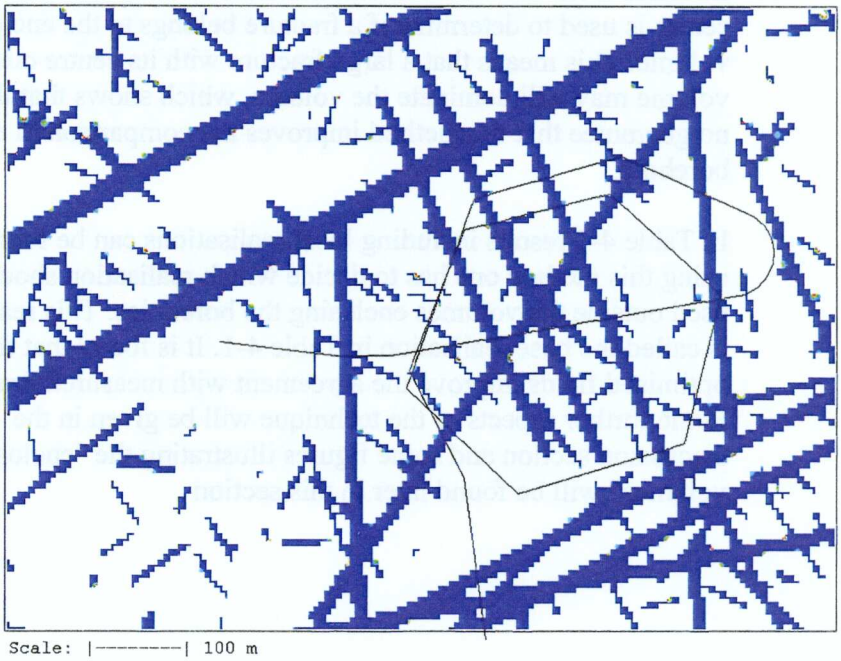

Figure 4-1. *Illustrations of calculated High Permeability Features. $T \geq 10^{-5}$ m^2/s (top) and $T \geq 10^{-6}$ m^2/s, all for a depth of 450 metres.*

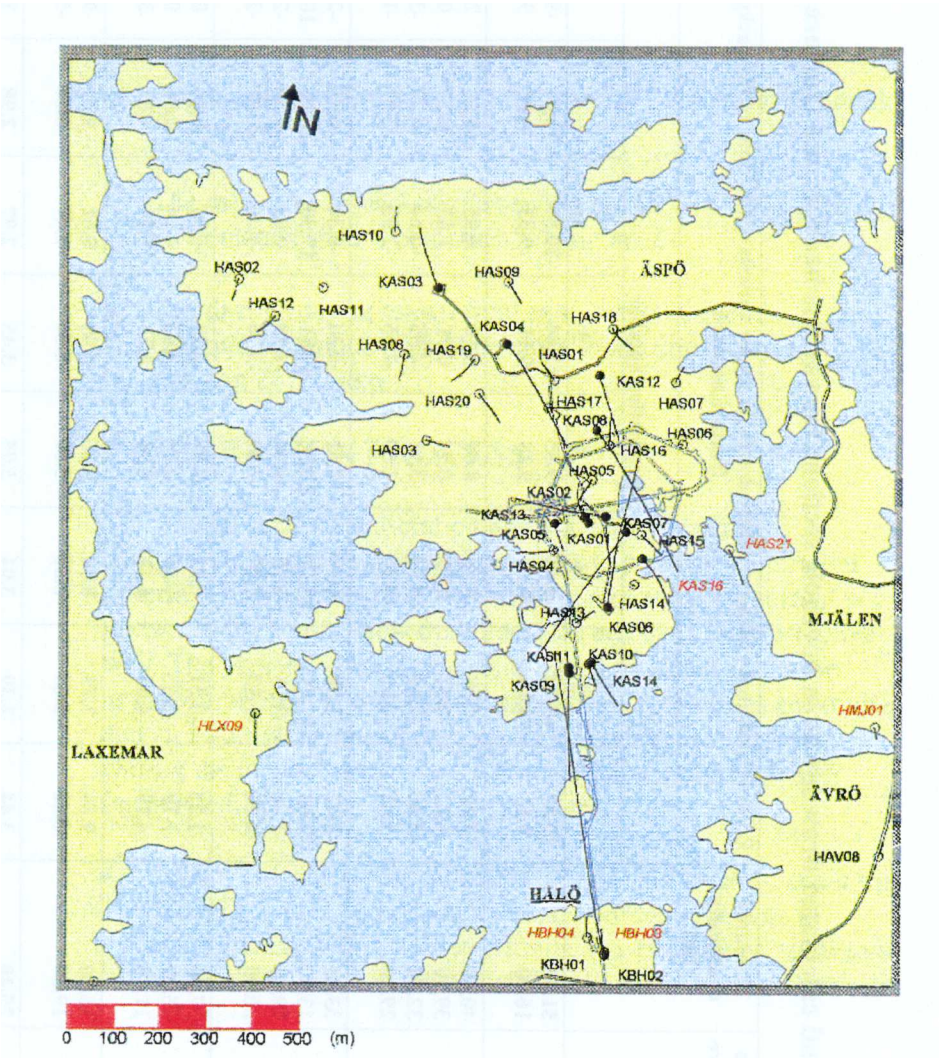

Figure 4-2. *Boreholes in the Äspö area.*

Table 4-1. Measured and calculated drawdowns in borehole sections for various background fracture networks. Tunnel front at position 2875 metres.

Borehole section	Contact with major fracture zone	Measured drawdown (m)	Error (Calculated - Measured drawdown) (in m) for various realisations of the background fracture network								Best	With local realisations.	
			Realisation number									Base realisation	
			1	2	3	4	5	6	7	8		1	4
K02-B4	no	51.50	-10.57	-9.79	-8.48	-9.85	-11.64	-10.89	-11.01	-9.92	3	-10.11	-9.38
K02-B3	yes	16.90	9.13	9.16	9.20	9.28	9.11	9.02	8.92	9.22		9.17	9.26
K05-E4	no	40.40	4.40	5.15	6.48	4.66	5.10	6.95	10.59	2.28	8	3.69	1.99
K05-E3	no	39.90	-2.22	-0.51	0.73	-0.74	0.71	1.83	-0.37	0.93		-0.56	0.41
K05-E2	no	32.50	-3.40	-2.14	-4.84	-3.61	-4.55	-4.64	-4.77	-3.13		-2.90	-3.44
K05-E1	yes	29.20	-1.41	-0.96	-3.36	-1.59	-2.56	-2.99	-3.09	-1.88		-1.58	-2.20
K06-F4	no	33.80	-2.42	-1.60	-0.68	-0.81	-0.24	-0.34	-0.95	-2.10	4	-1.11	-0.78
K06-F3	no	13.90	15.84	17.64	18.12	15.24	19.81	17.30	16.21	18.38		14.57	15.99
K06-F2	no	29.10	-1.70	0.35	-0.78	-1.44	-1.29	0.83	-1.46	-2.13		-2.82	-1.41
K06-F1	yes	30.00	-4.26	-1.13	-2.97	-2.82	-3.76	-1.20	-3.42	-2.91		-4.30	-3.35
K07-J4	no	37.50	-1.23	-0.51	-0.01	-2.07	-0.23	-5.97	0.08	0.72	8	0.68	1.09
K07-J3	no	25.20	1.78	-0.55	-0.59	-1.75	-1.42	4.04	3.86	0.20		0.65	0.83
K07-J2	yes	11.70	4.79	4.45	4.41	4.08	4.33	5.39	4.02	3.80		3.93	3.81
K08-M2	no	16.60	9.59	7.75	8.04	9.25	6.08	9.61	9.27	9.31	5	7.44	6.80
K08-M1	yes	19.50	-5.55	-5.69	-5.58	-5.59	-5.56	-5.47	-5.50	-5.60		-5.40	-5.45
K12-DC	no	25.40	3.44	2.39	3.04	3.05	3.45	2.97	2.98	1.89	1	3.52	3.47
K12-DB	no	25.30	2.31	3.39	3.17	3.26	3.63	3.97	2.62	5.09		2.61	2.30
K12-DA	yes	24.90	2.38	4.09	3.63	3.10	3.86	4.07	3.43	4.48		3.10	2.85
K16-3	no	28.00	-6.61	-6.68	-6.50	-7.72	-6.56	-5.73	-8.28	-7.04	6	-5.97	-5.77
K16-2	yes	18.60	-6.43	-6.48	-6.28	-6.51	-6.45	-6.28	-6.40	-6.48		-6.39	-6.41
K16-1	no	16.70	-5.59	-6.09	-4.79	-5.70	-4.87	-5.01	-5.04	-5.36		-5.59	-5.28
	Mean error		0.11	0.58	0.57	0.08	0.33	0.83	0.56	0.46		0.12	0.25
	Goodness of fit		6.32	6.29	6.40	6.20	6.76	6.75	6.80	6.54		5.86	5.84

Conductivity on a 3 metres scale. In order to collect statistics for the 3 metres scale a smaller computational domain was used, see Figure 1-1. The depth interval chosen was 200 to 500 metres. The block is thus 300 x 300 x 300 m^3 and with $\Delta = 3$ metres we get 10^6 cells in the grid. Isolated fractures were not removed for this case, as this was considered to be closer to the experimental conditions. As can be seen in Table 4-2, where the number of fractures generated are given, fractures down to a size of 2.5 metres were considered. The reason for this is that the gridsize was reduced to 3 metres.

Comparisons with field data are given in Figure 4-3, where it can be seen that the conductivity distribution based on this fracture network has 36% of the cells with a conductivity of less than 10^{-11} m/s. A minimum conductivity of 10^{-12} m/s was prescribed to all cells. The calculated distribution is not in agreement with the field data. However, adding a lognormally distributed conductivity with $mean(\log_{10}(K)) = -10.0$ and *std. dev* $(\log_{10}(K)) = 0.8$ to all cells gives a much better agreement with field data. It should be noted that adding this conductivity field does not strongly influence the drawdown calculations, nor the frequency of high permability features, presented above. It may however prove important to have also the "low conductivity connections" well described when transport simulations are attempted. The field data are based on measurements in boreholes with a packer spacing of 3 metres. It may be questioned if it is relevant to compare these data with gridcell conductivities, with $\Delta = 3$ metres. If, as an example, we assume that the radius of influence is 3 metres in the field measurements we sample a cylinder with diameter 6 metres and length 3 metres. In order to see the influence of the cell size the distribution for $\Delta = 5$ metres (using the laboratory model domain) was also calculated. The result is shown in Figure 4-3. It is found that the conductivity distribution for $\Delta = 5$ metres is perhaps closer to the field data. Considering this uncertainty about the sampled volume, it is probably not worthwhile to strive for a closer agreement with the measured distribution.

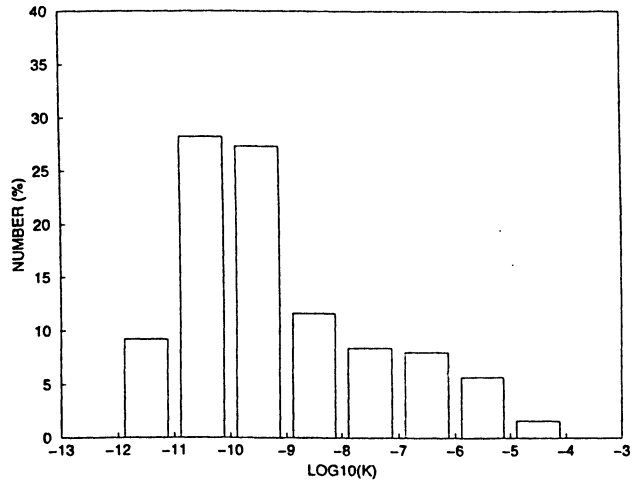

Measured
(Rhén et al., 1997)

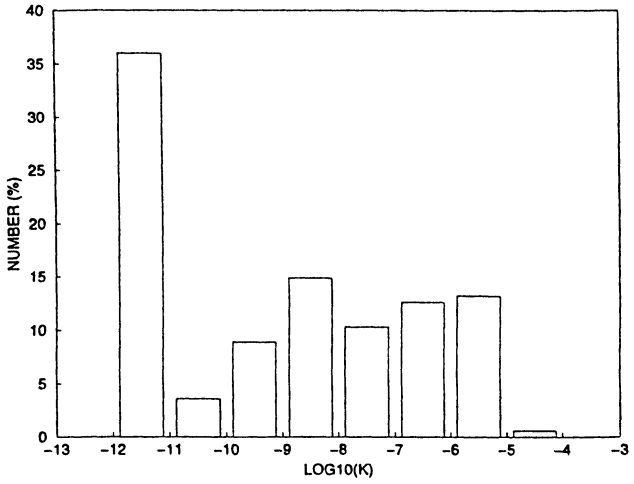

Simulated
l_{min} = 2.5 m

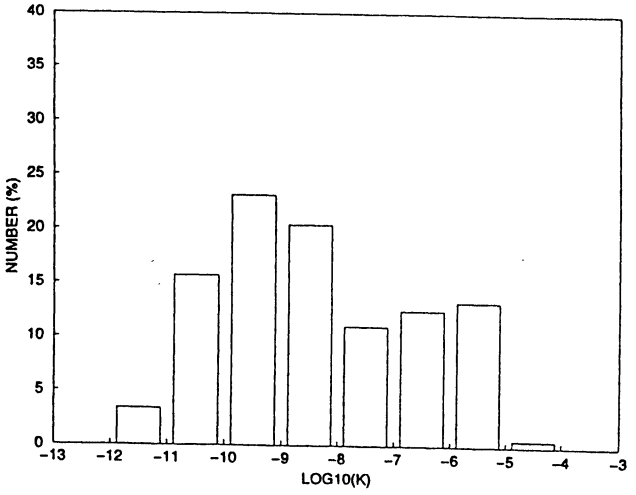

Simulated
l_{min} = 2.5 m
Background
conductivity
added.

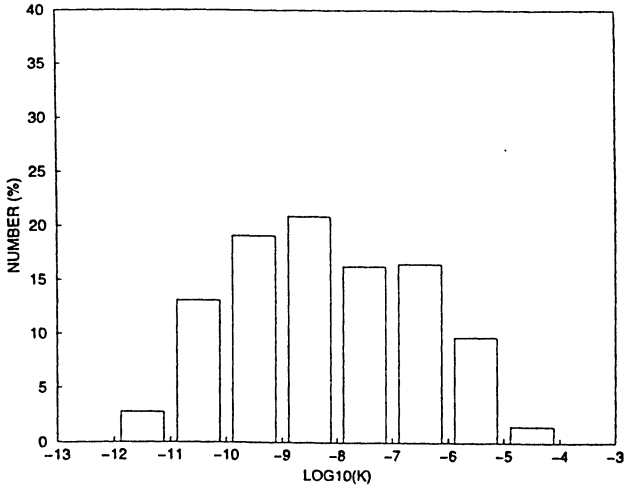

Simulated
l_{min} = 5.0 m
and Δ = 5.0 m
Background
conductivity
added.

Figure 4-3. *Measured and simulated conductivity distributions on a 3 metres scale and simulated distribution for 5 metres scale.*

Equivalent conductivity. Finally the comparison with the conductivity field from the site model is discussed. The equivalent conductivity for the present block, using data from the site model, was calculated with a Δ of 20 metres as this was the gridsize used in the site model. With the method used to generate conductivities in the site model one can not expect the equivalent conductivity to be grid independent, i.e. we have to use the gridsize that was used in the calibration of the site model. For the new method it is expected that the best result is obtained with the finest possible gridsize and that the result should be only weakly dependent on the gridsize. Calculations with the new method was therefore performed with $\Delta = 5$ metres. Results are found in Table 4-3. The agreement is considered to be good, for all three directions.

Table 4-2. Background fractures for simulation with $\Delta = 3$ metres.

Fracture set number	Length interval [m]	Numbers generated
1	160-320	15
2	80-160	19
3	40-80	69
4	20-40	360
5	10-20	1 781
6	5-10	9 563
7	2.5-5	52 547

Table 4-3.Comparison between equivalent conductivities from the site-model, Svensson (1997b), and the present model.

Direction	Equivalent conductivity $*10^{-7}$ m/s	
	Data from site-model	Present model
West-East	0.76	0.74
South-North	1.12	1.52
Low-High	4.49	4.77

4.5 SOME FURTHER COMPARISONS WITH DATA

In this section we will analyse the generated conductivity field and, when possible, compare with data. The results were not directly used in the calibration process but are anyway believed to add confidence to the generated fields.

The first topic to be discussed is heterogeneity. As there is a large contrast in the hydraulic conductivity between fractures and intact rock, it is of interest to compare the heterogeneity of the generated conductivity field with field data. This can be done (Painter, 1999) by comparing the histograms of the increments in $\log K$, as shown in Figure 4-4. The basic idea is to determine the probability of finding a certain difference in $\log_{10} K$ when moving vertically a certain distance (the "lag" in Figure 4-4). Obviously, if we had a smoothly varying conductivity field the probability to find large increments for short lags would be low. The field data shown in Figure 4-4 are from 3 metres packer tests in eight bore-holes on Äspö (see Rhén et al., 1997). These data were analysed, with respect to heterogeneity, by Painter (1999).

An illustration of the heterogeneity of the generated conductivity field is given in Figure 4-5. The cell conductivity, with $\Delta = 5$ metres, along a horizontal line is shown. The line is parallel to the final part of the tunnel, at the same depth, but roughly 100 metres south of the Äspö tunnel. Exact coordinates for the line are: $x = 1837$ to 2037 metres, $y = 7172.5$ metres and $z = 447.5$ metres; all in the Äspö coordinate system. The reason for sampling this volume is that conductivity measurements, with 5 metres spacing, have recently been carried out in this volume, see Follin et al. (1998). It is clear from Figure 4-5 that large variations in K from cell to cell is a characteristic feature of the conductivity field generated. Qualitatively the distribution is in good agreement with the above mentioned measurements.

An often used parameter to characterise a fracture network is the fracture area per unit volume, P_{32}. In Table 4-4 the contributions from different fracture sets are given. As can be seen, P_{32} is depending on the cut-off length in the fracture network. For the present cut-off length, 5 metres, the P_{32} parameter is 0.086. If however $l_{cut-off}$ was 2.5 metres P_{32} would increase to 0.117, and if $l_{cut-off}$ was 0.5 metres P_{32} would be 0.35; all based on the power-law distribution used. Follin and Hermansson (1996) summarised reported estimates based on Äspö data. They found P_{32}-values in the range 0.0664 to 2.0 m^2/m^3. This is a wide range which however includes the estimates from the present model.

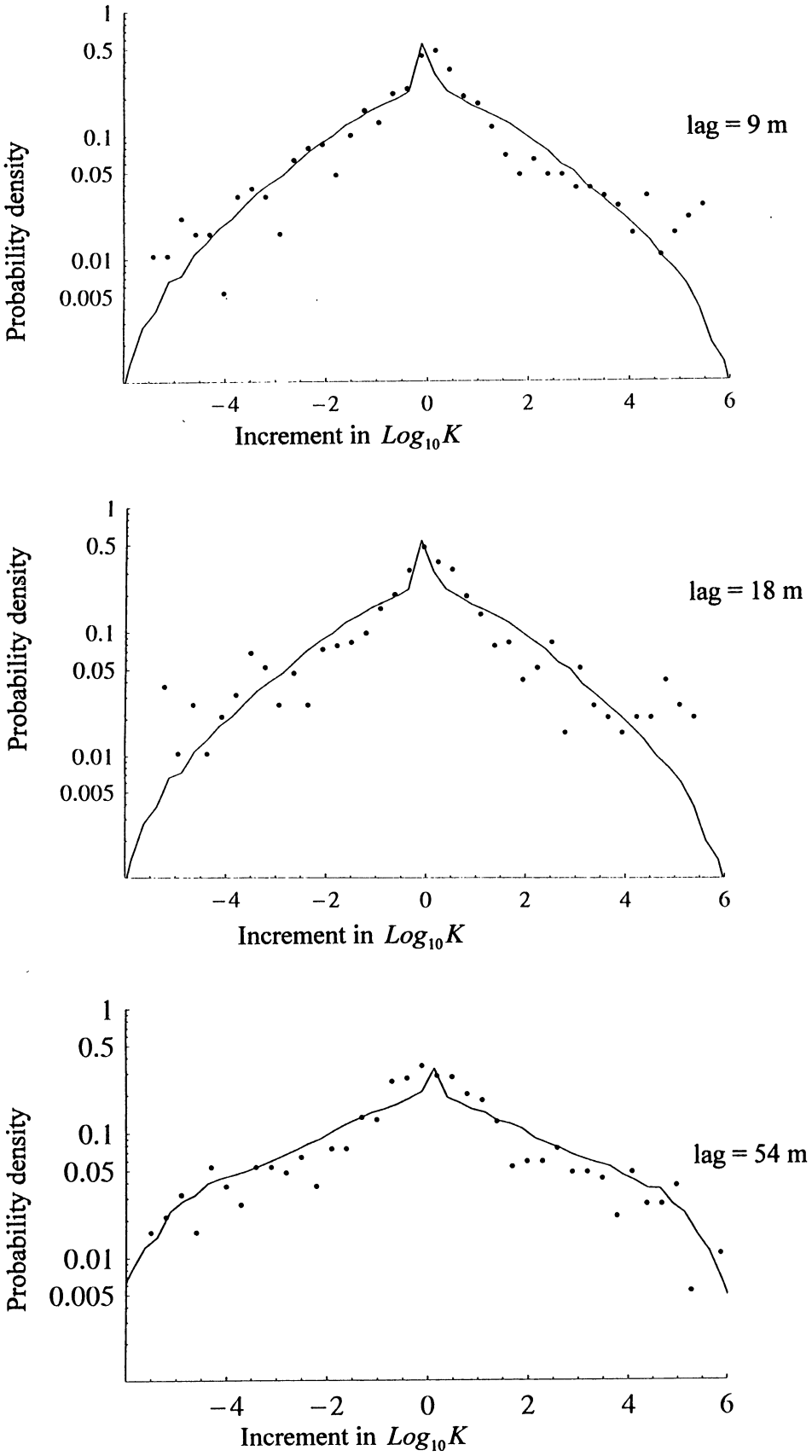

Figure 4-4. *Increment histograms. Measured (•) versus simulated (-) probability distribution for different lags.*

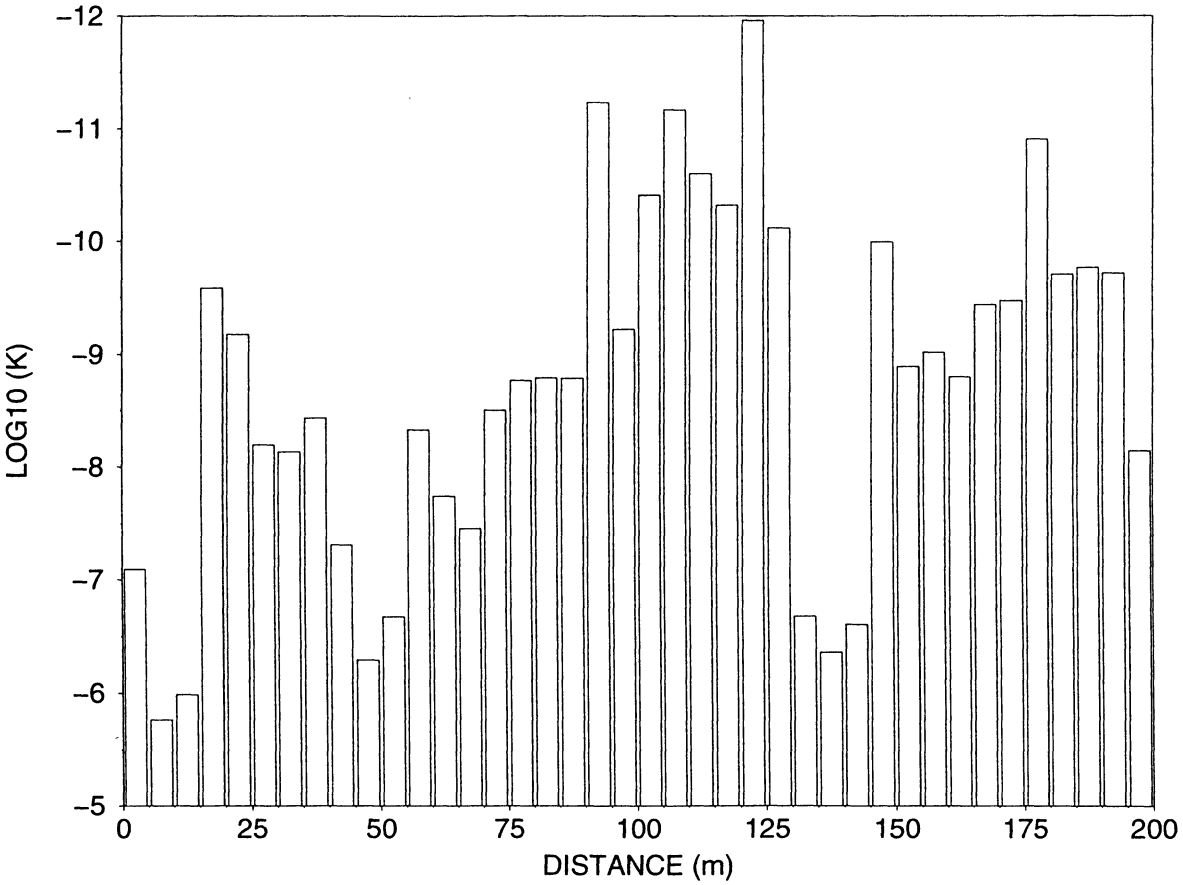

Figure 4-5. *Conductivity distribution along an east-west line south of the final part of the Äspö tunnel. The conductivity in the north-south direction is shown, but other directions are similar.*

Table 4-4. The fracture intensity P_{32}, expressed as m^2/m^3, based on deterministic fractures and the background fracture network.

Fracture length interval	P_{32} [m^2/m^3]
Determ. fracture zones	0.014
160-320	0.008
80-160	0.007
40-80	0.008
20-40	0.011
10-20	0.016
5-10	0.022
	Σ 0.086

4.6 CONCLUDING REMARKS

The main conclusion from this calibration exercise is that good agreement with Äspö data can be obtained by the following actions:

- Retain the transmissivities for the major fracture zones, as used in the site scale model, without modification.

- Employ a background fracture network as specified in Table 3-2, and with a fracture transmissivity that decreases with fracture size, see equation (4-1).

- Add a background cell conductivity which has a lognormal distribution. Also apply a lower limit ($=10^{-12}$ m/s) for the cell conductivity.

When comparisons with measured drawdowns in borehole sections were made, it was found advantageous to use different realisations of the background fracture network for different boreholes. This is a novel technique which seems to work well, but may require some further evaluation. It needs, for example, to be demonstrated that the composite field has the same general statistical properties as a single realisation.

Two examples of the resulting conductivity fields are given in Figure 4-6. Two base realisations are used, but the realisations around the boreholes are in both cases from the optimum realisation, see Table 4-1. The rectangles in Figure 4-6 indicate the enclosing volumes. In the vertical the volumes extended from the top to the bottom of the domain. By studying the same rectangle in both figures, one can see that small fractures inside the two rectangles are the same.

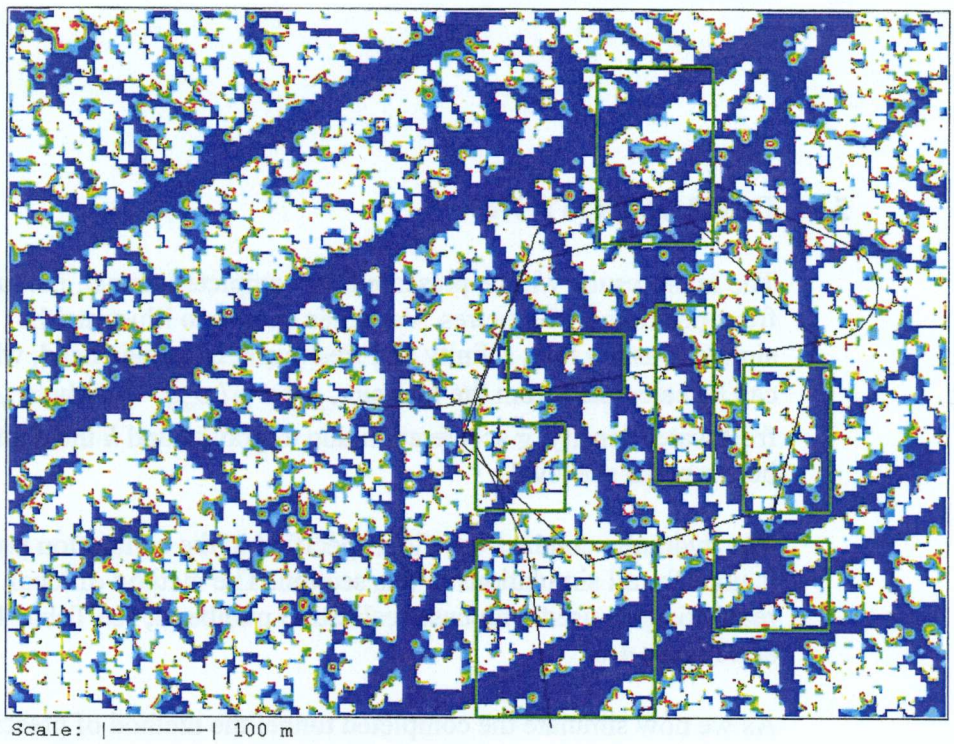

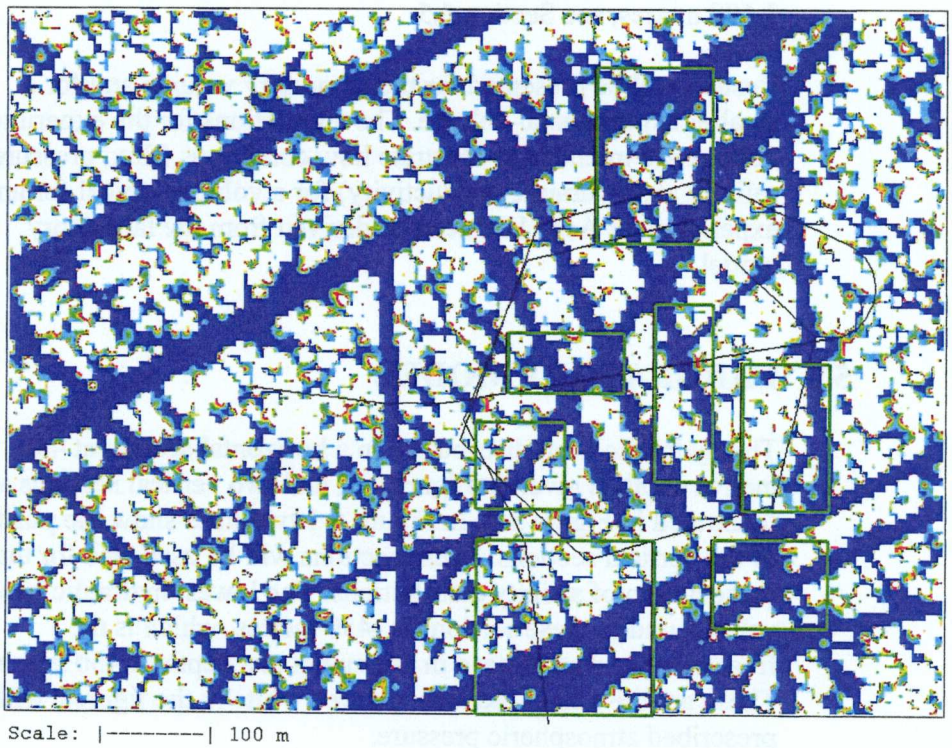

Figure 4-6. *Conductivity fields for base realisations 4 (top) and 1, see Table 4-1. The rectangles indicate volumes where fractures are taken from the optimum realisation.*

$$\text{Conductivity interval}: \begin{cases} \text{blue} > 10^{-8} \text{ m/s} \\ 10^{-8} < \text{red} < 10^{-9} \text{ m/s} \end{cases}$$

5 MAIN RESULTS

5.1 INTRODUCTION

The main results will be presented for completed tunnel, i.e. tunnel front position 3 600 metres. Variables chosen to illustrate the simulations are flux, salinity and freshwater hydraulic head, which can be calculated from the pressure, p, as $p/\rho_o g - h$, where ρ_o is freshwater density, g acceleration due to gravity and h the depth below mean sea level.

The hydraulic conductivity field specified in the calibration process is used for all simulations in this section. The method of local realisations is used with base realisation number 4, see Table 4-1 and Figure 4-6.

As we now simulate the completed tunnel the method of prescribed pressure in the tunnel will be used for tunnel section 3 100 to 3 600 metres, see Section 3.5.

Results will be presented for the laboratory volume and for a smaller experimental volume. The simulations for the experimental volume are intended to illustrate how conditions (flux, pressure, salinity and hydraulic conductivity) for a volume typical for an experiment at Äspö HRL can be derived from the laboratory model.

5.2 LABORATORY MODEL

The hydraulic head distribution in a horizontal section at 450 metres depth is given in Figure 5-1, and two vertical sections are illustrated in Figure 5-2. In Figure 5-1 two lines show the positions of the vertical sections. These sections will be used also for the presentation of salinity distributions. The lowest hydraulic head value found in these sections is -450 metres, which is the freshwater hydraulic head in the tunnel at a depth of 450 metres. These are the tunnel sections, marked white in the figures, with prescribed atmospheric pressure.

The salinity distribution in the same sections can be found in Figures 5-3 and 5-4. The general impression from these figures is that the tunnel generates a strong vertical flow which brings up water with very high salinity into the tunnel area.

Horizontal flow distributions at various depths are shown in Figures 5-5 to 5-8. Figure 5-5 gives the flow at a depth of 230 metres; this is the depth for the first crossing of fracture zone NNW7 with the tunnel. From the enlarged view one can however see that also the inflow to the elevator shaft has a strong influence on the flow pattern. The next depth illustrated, see Figure 5-6, is 300 metres. At this depth the tunnel crosses NNW1 and NNW2 in the southern part of the first turn of the spiral. Figure 5-7 gives the flow at 395 metres depth, which is at the bend in the tunnel. Of the two inflows from NNW4 seen, one is thus above this level and one is below. Conditions at 450 metres depth can be studied in Figure 5-8.

Flow and salinity distributions in fracture zones NNW1 and NNW4, can be found in Figures 5-9 and 5-10. The location of these fracture zones is given in Figure 3-1. The upconing of salt water, due to the tunnel inflows, is well illustrated in Figure 5-9, which gives the salinity in NNW1, with a view from west. Conditions in NNW4 can be studied in Figure 5-10, now with a view from east. Flow vectors in the two figures may have a component perpendicular to the fracture zone, particularly where other zones cross, and a scale for the flux vector is therefore not given.

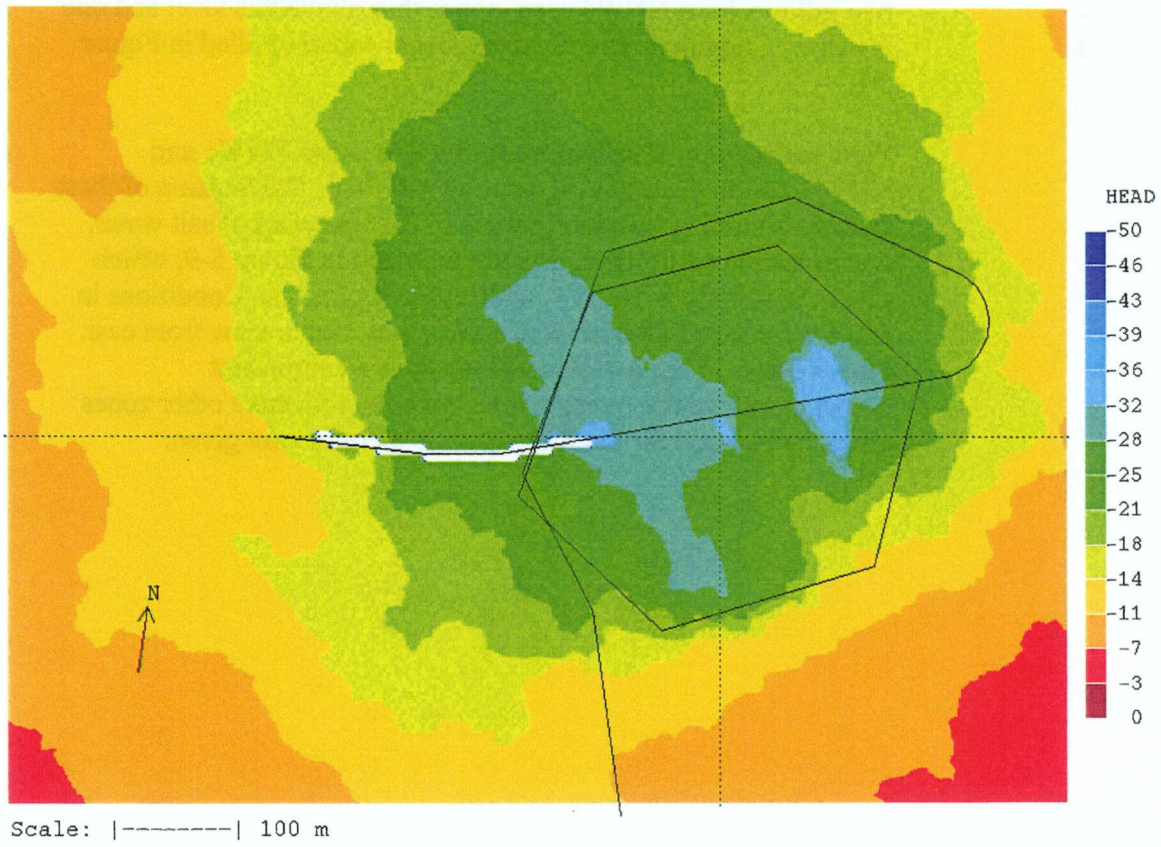

Figure 5-1. *Hydraulic head distribution at a depth of 450 metres below ground level. The two lines show positions for vertical sections. White areas mark tunnel sections with atmospheric pressure.*

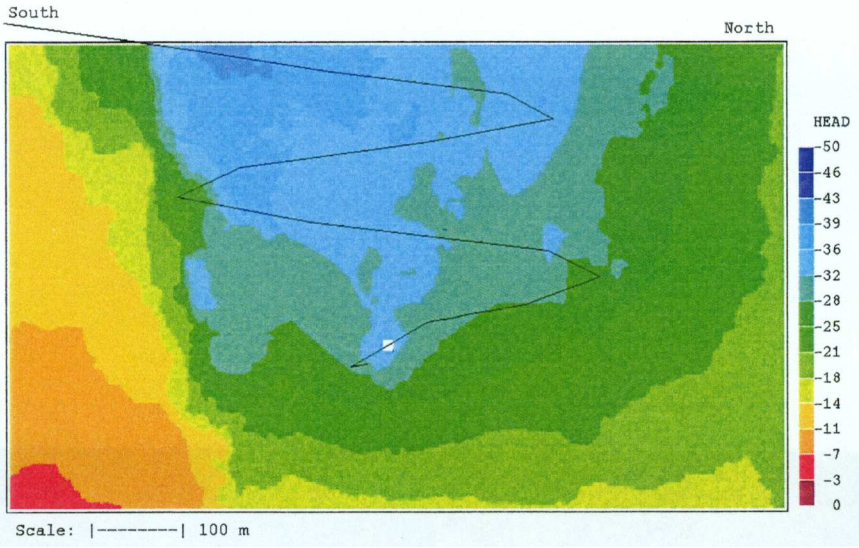

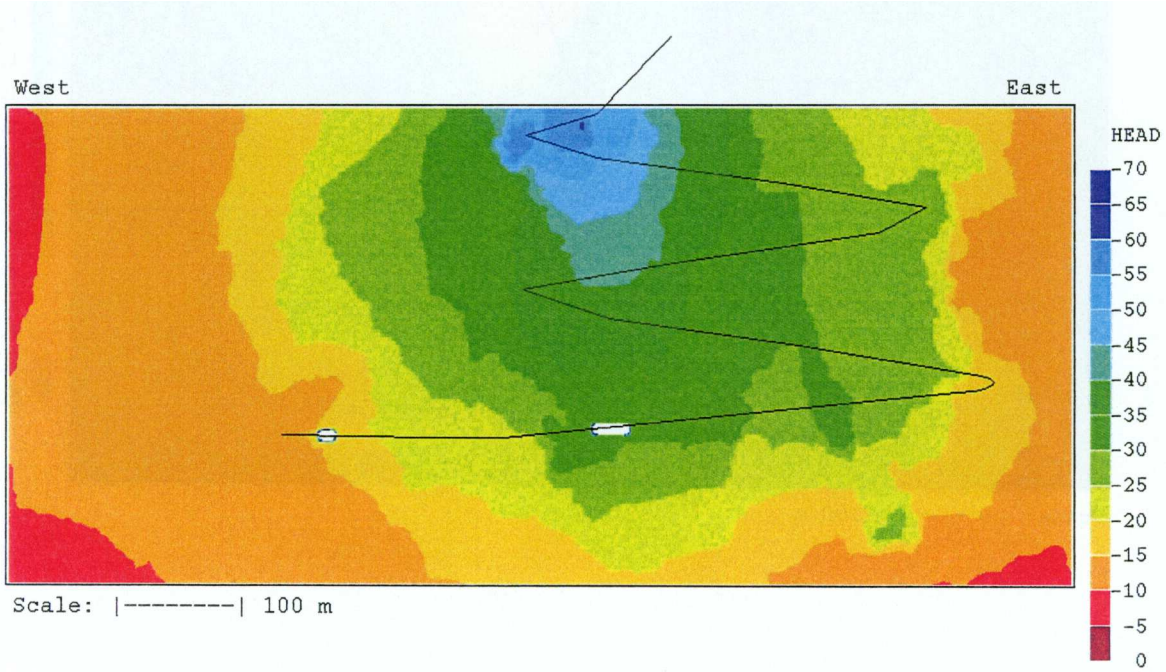

Figure 5-2. *Hydraulic head in two vertical sections (positions shown in Figure 5-1). White areas mark tunnel sections with atmospheric pressure.*

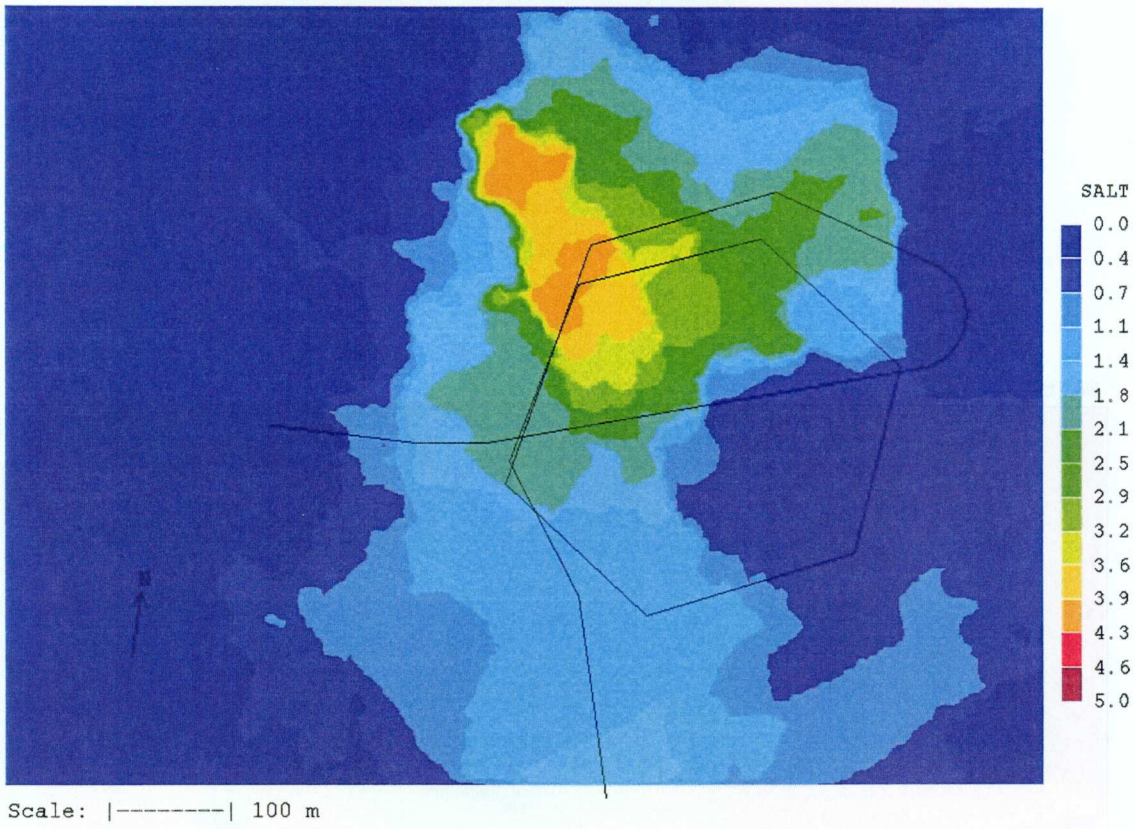

Figure 5-3. *Salinity (in %) distribution at a depth of 450 metres below ground level.*

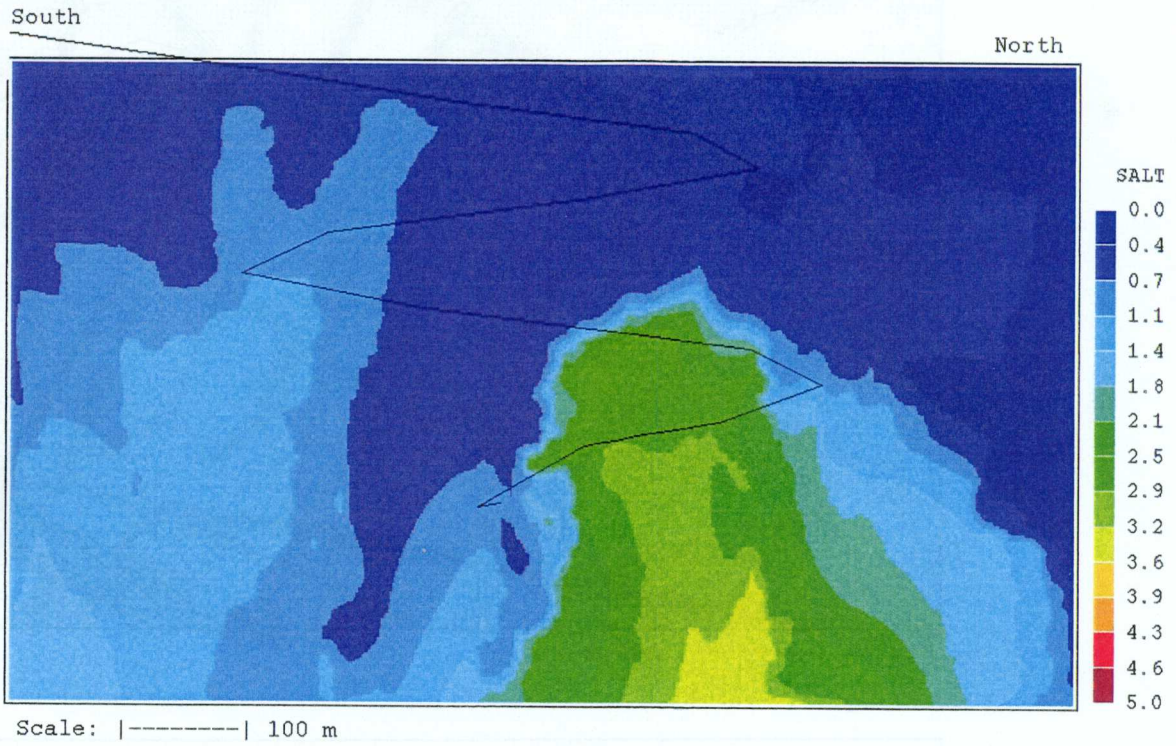

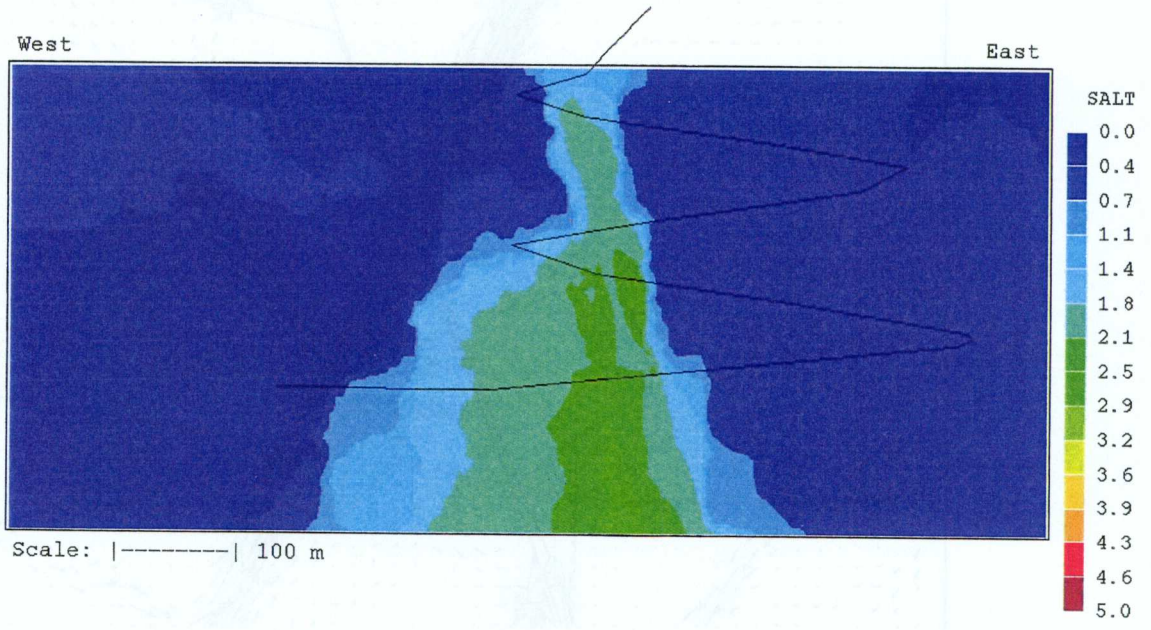

Figure 5-4. *Salinity (in %) distribution in two vertical sections (positions shown in Figure 5-1).*

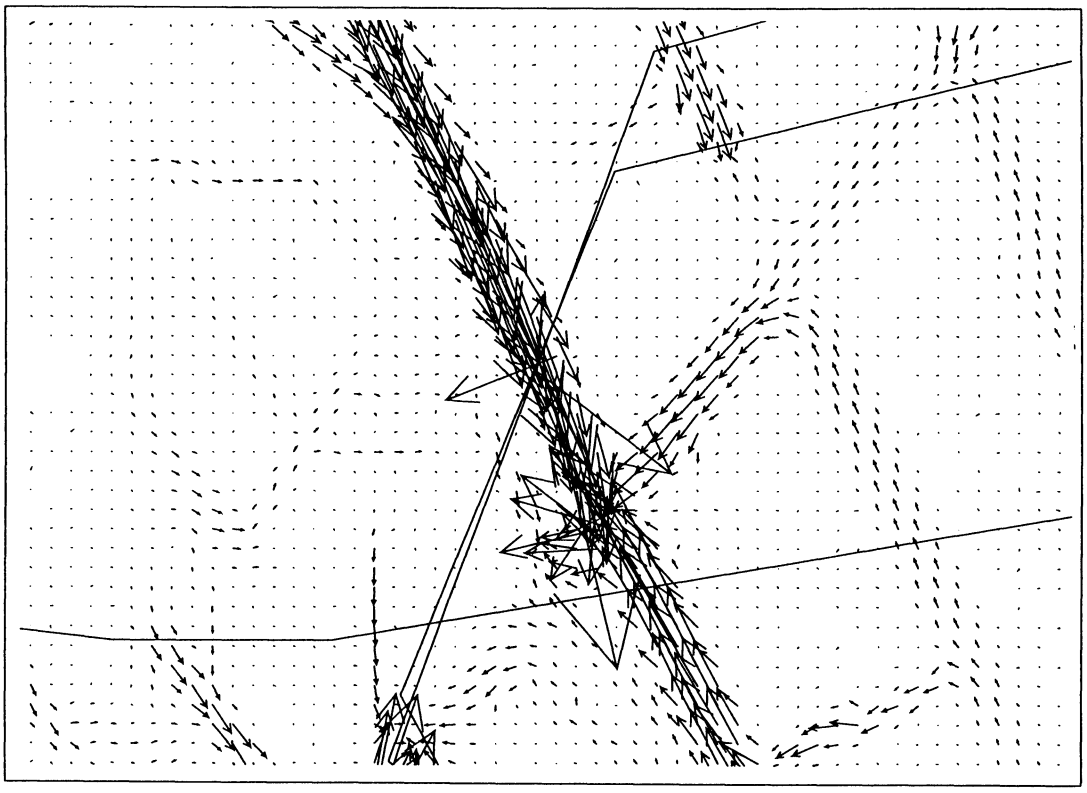

ENLARGEMENT

Figure 5-5. *Horizontal flow at a depth of 230 metres below ground level.*
Darcy velocity scale: ⟶ 5×10^{-7} *m/s (top figure).*

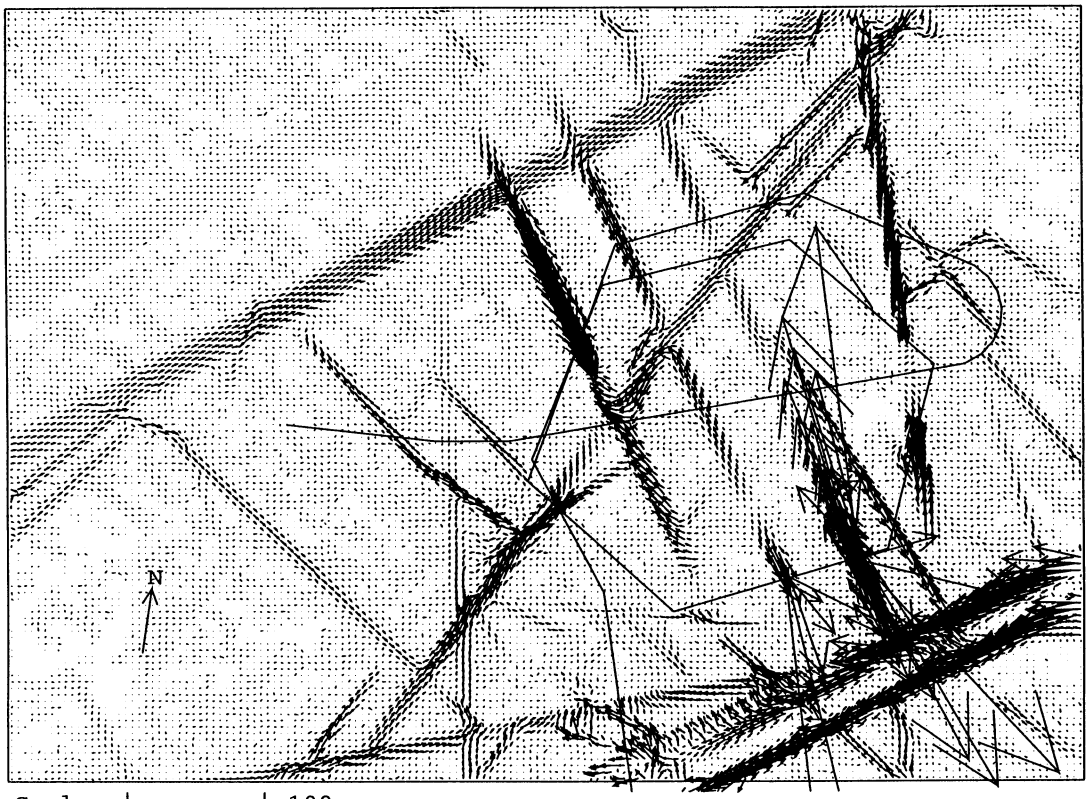

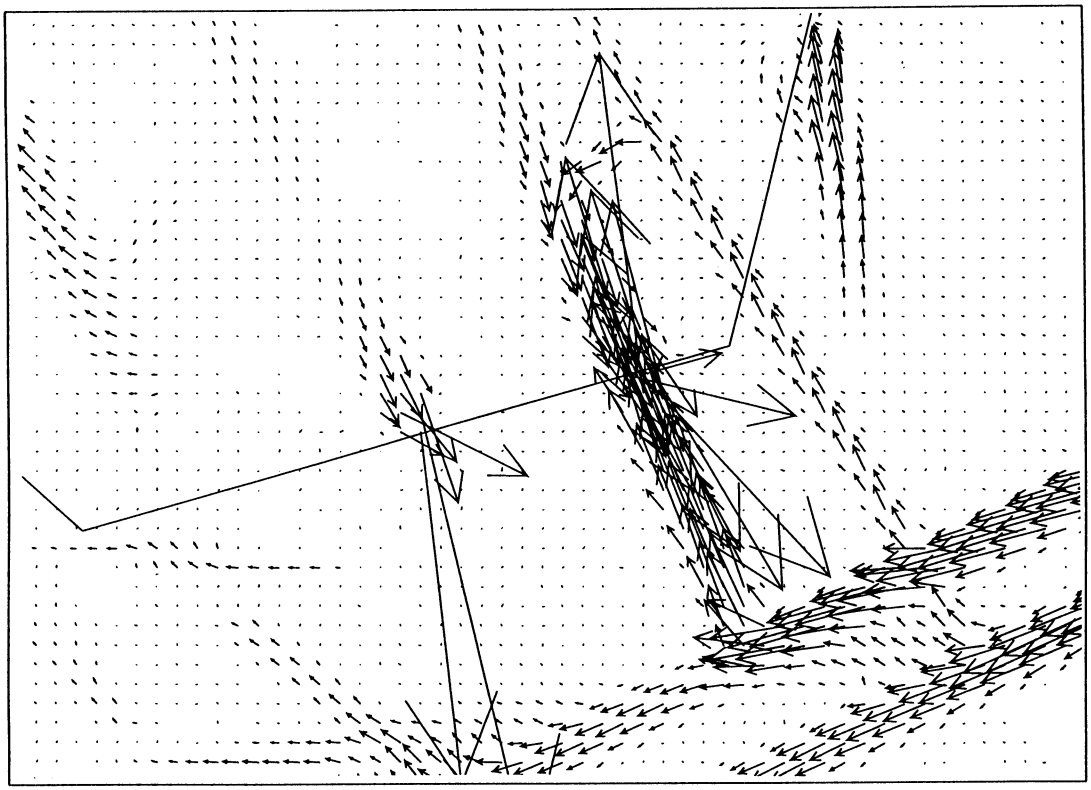

ENLARGEMENT

Figure 5-6. *Horizontal flow at a depth of 300 metres below ground level.*
Darcy velocity scale: ⟶ 5×10^{-7} *m/s (top figure).*

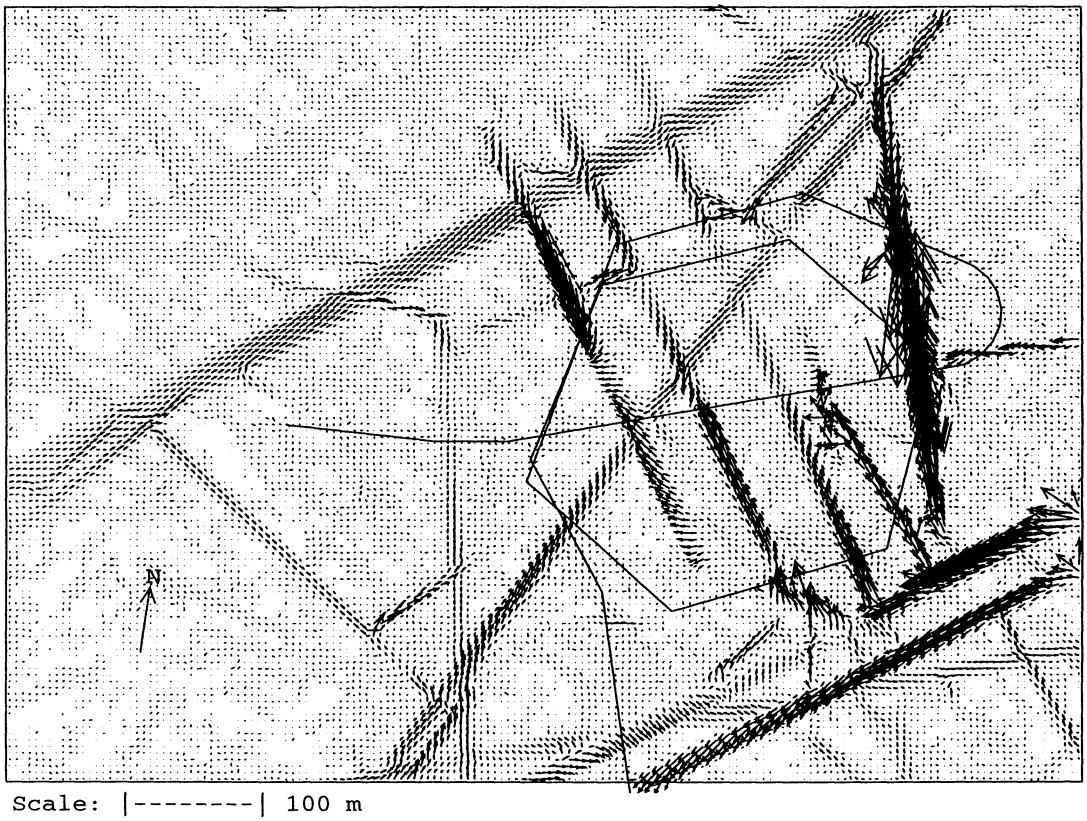

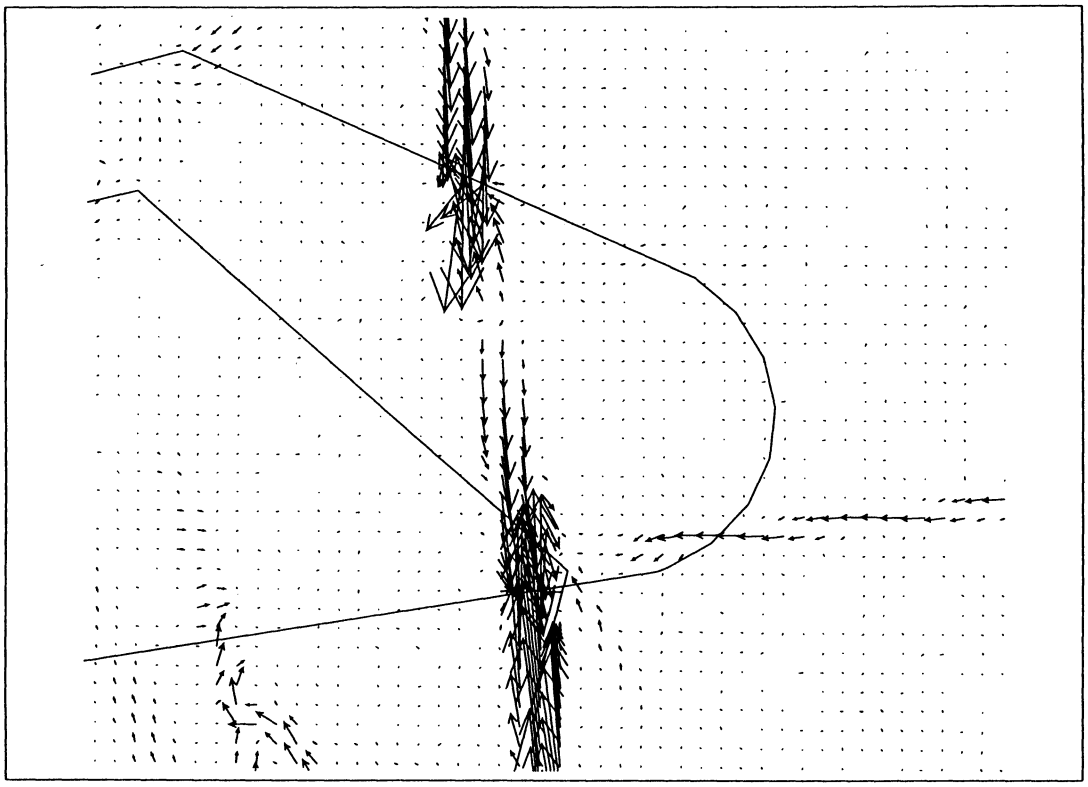

ENLARGEMENT

Figure 5-7. *Horizontal flow at a depth of 395 metres below ground level.*
Darcy velocity scale: ⟶ 5×10^{-7} *m/s (top figure).*

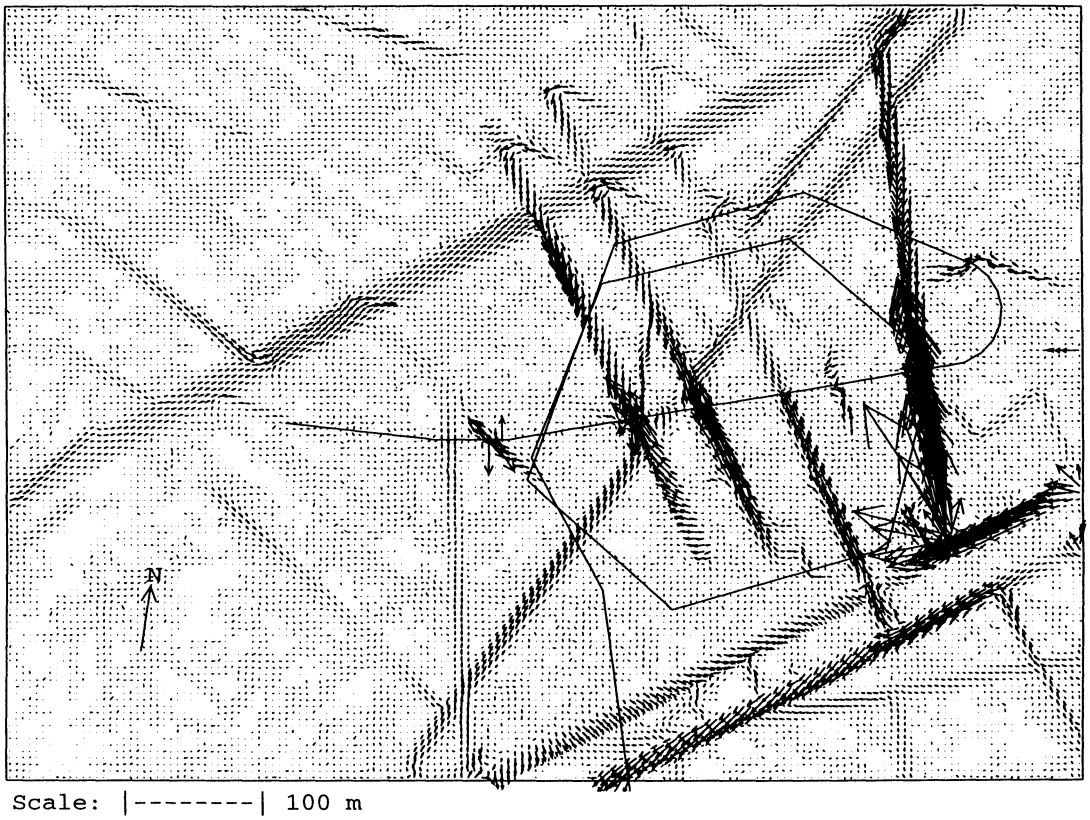

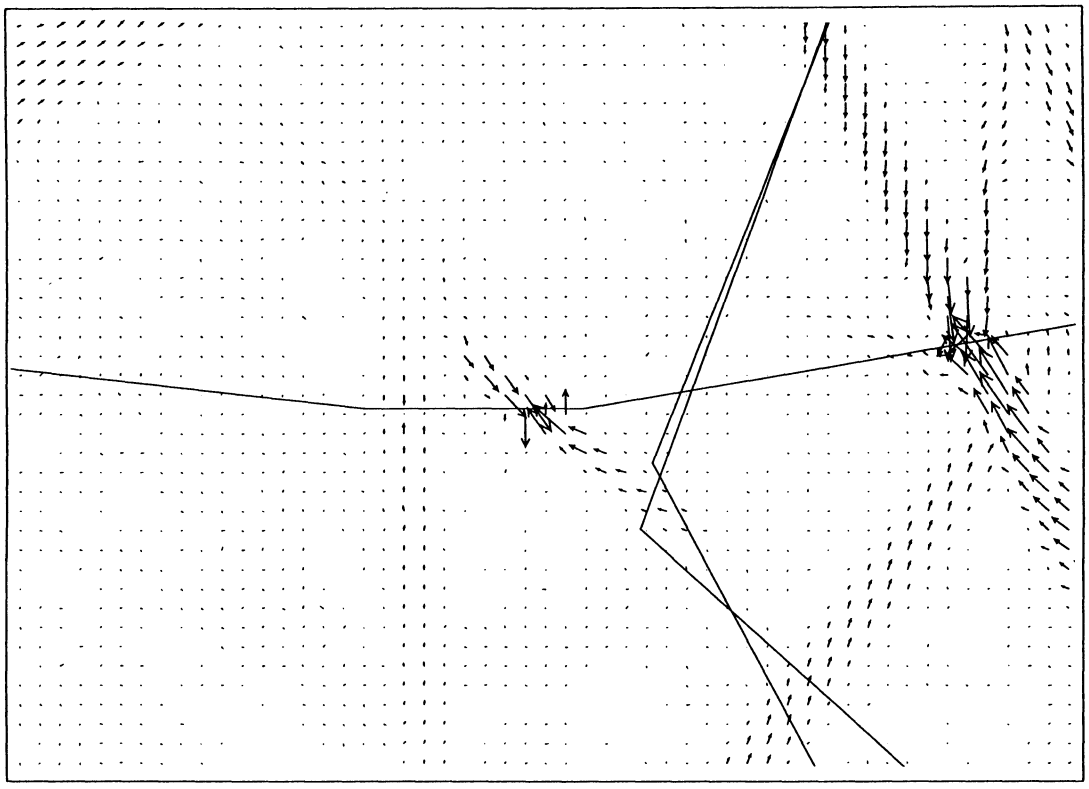

ENLARGEMENT

Figure 5-8. *Horizontal flow at a depth of 450 metres below ground level.*
Darcy velocity scale: ⟶ 5×10^{-7} *m/s (top figure).*

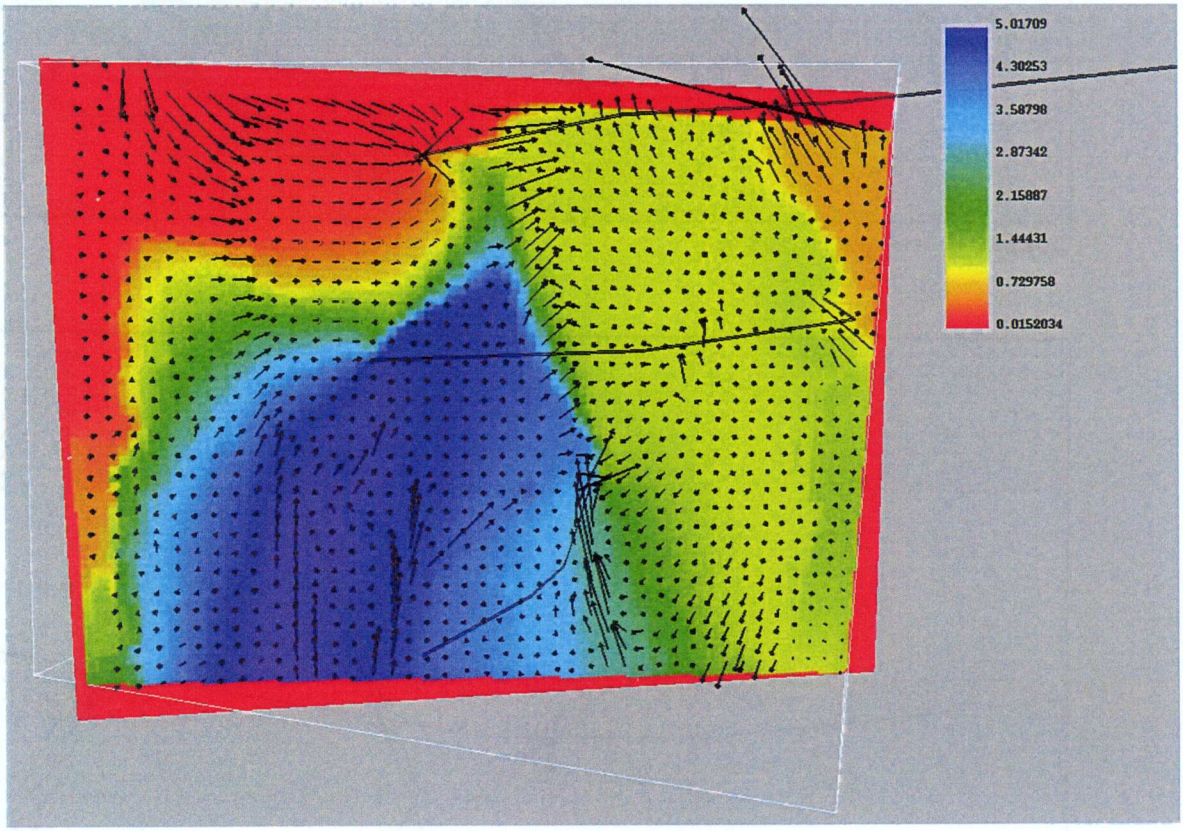

Figure 5-9. *Flow and salinity (in %) distribution in NNW1. View from west.*

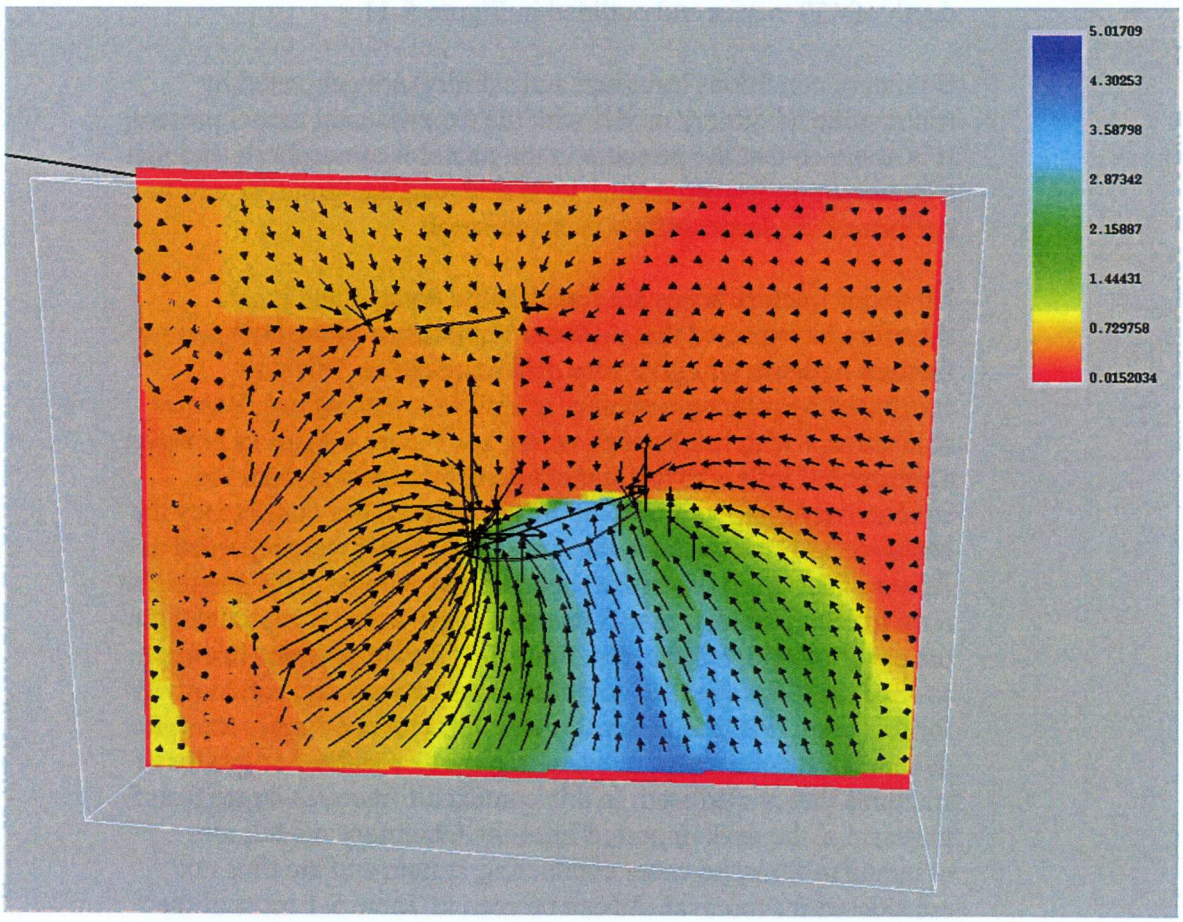

Figure 5-10. *Flow and salinity (in %) distribution in NNW4. View from east.*

5.3 EXPERIMENTAL VOLUME

As already mentioned, the results for the experimental volume are intended to illustrate how the laboratory model can be used to characterise a smaller volume close to the main tunnel. It is thus not a real experimental volume.

The volume chosen is shown in Figure 5-11. Horizontal dimensions are 80 x 80 metres and the vertical dimension is 50 metres (425 to 475 metres below ground level). The gridsize is 1 metre in all three directions. It is further supposed that a tunnel, with a cross-section of 5 x 5 metres is excavated for the experiment. The tunnel is at a depth of 450 metres and outlined in Figure 5-11.

Boundary conditions (pressure and salinity) are generated by running the laboratory model with the experimental tunnel present. It is assumed that the pressure in the tunnel is atmospheric and that a maximum inflow of about 1 l/s is accepted, i.e. grouting will be performed if a larger inflow is encountered.

No major fracture zones are found in the domain and it can therefore be expected that different realisations of the background fracture network will give very different results. This was confirmed by running a number of different realisations. Base realisation 4 with local optimisation, see Figure 4-6, gives however a substantial inflow to the tunnel as can be expected from the conductivity distribution (to be shown below). For consistency the background fractures from the laboratory model were regarded as deterministic fractures in the experimental volume. This means that only fractures smaller than 5 metres are generated stochastically in the experimental volume, see Table 5-1. As we generate fractures as small as 0.6 metres we do not add any background conductivity for this case. It is thus assumed that all fractures of importance are generated. It is then also relevant to remove fractures or groups of fractures that are isolated. In this context all fractures larger than 5 metres, i.e. the ones imported from the laboratory model, are assumed to form the water conducting system and are thus not considered for removal. As can be seen in Table 5-1 most of the smaller fractures are isolated and hence removed. The resulting conductivity fields, at a depth of 450 metres, are shown in Figure 5-12.

Hydraulic head and salinity distributions are given in Figure 5-13 and the flow distribution in Figure 5-14. It is clear that nearly all the inflow, which is about 1.1 l/s, is through the large fracture zone in the north-east part of the domain.

Table 5-1. Background fracture network for experimental volume.

Fracture set	Length interval [m]	Number of fractures generated	Number of fractures isolated
1	2.5-5	1 092	685
2	1.25-2.5	6 325	5 380
3	0.6-1.25	42 713	35 774
		Σ 50 130	Σ 41 839

The purpose of the simulation of an experimental volume is to illustrate a possible use of the laboratory model. Hopefully this has been achieved. The exercise does however also point to some questions that need to be addressed if realistic simulations are attempted. For example:

- What is the smallest fracture size that should be regarded as belonging to the deterministic system and hence be imported from the laboratory model? In the present study all fractures larger than 5 metres were imported from the laboratory model. If this is a good choice is however an open question.

- In an experimental volume a fracture mapping is often performed. The information gathered should be utilised in the generation of the fracture network; either in the statistical distributions used to generate the fracture system or simply by introducing major fractures as known deterministic fractures.

- A more theoretical question may also be of interest when an experimental volume is considered. It was found in this tentative simulation that the volume was not conductive, i.e. no inflow to the tunnel was generated, unless a fairly large fracture was present in the volume. This leads to the following question: if the largest fracture in the volume is l_{max} what is then the probability, $p(l_{max})$, that two opposite faces of the domain are connected? It is believed that the answer to this question provides an interesting characterisation of a rock volume.

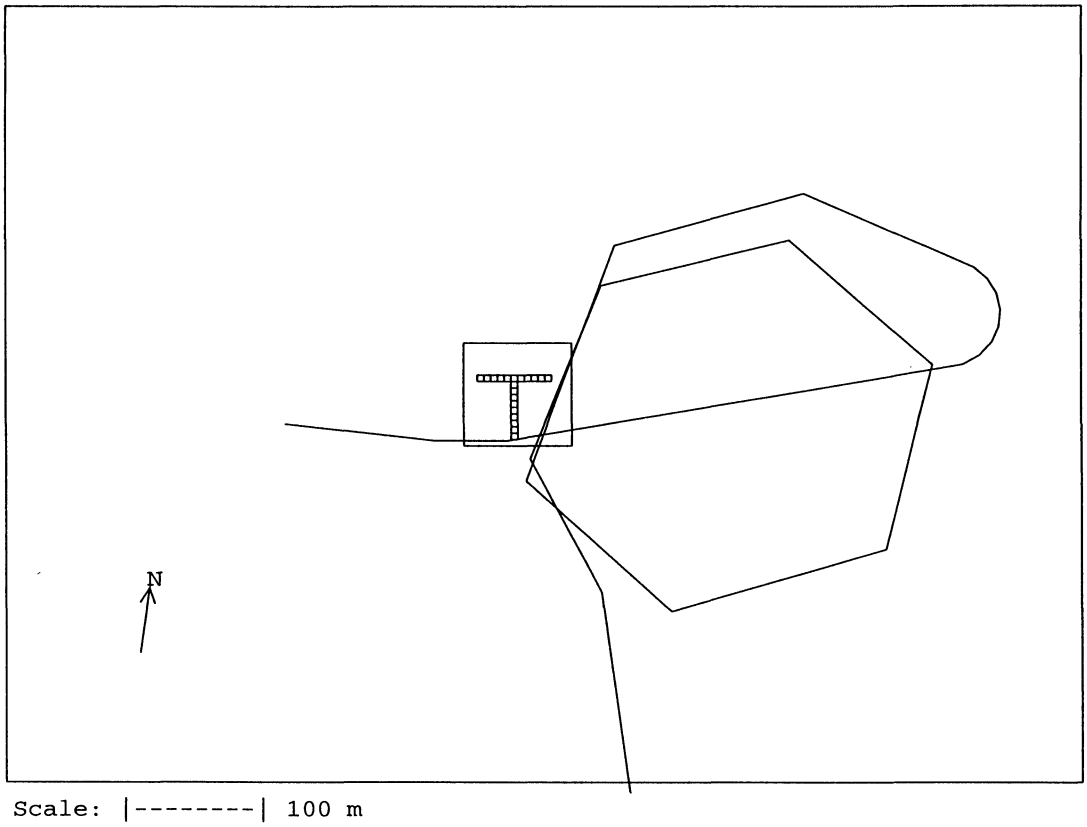

Figure 5-11. *Location of experimental volume.*

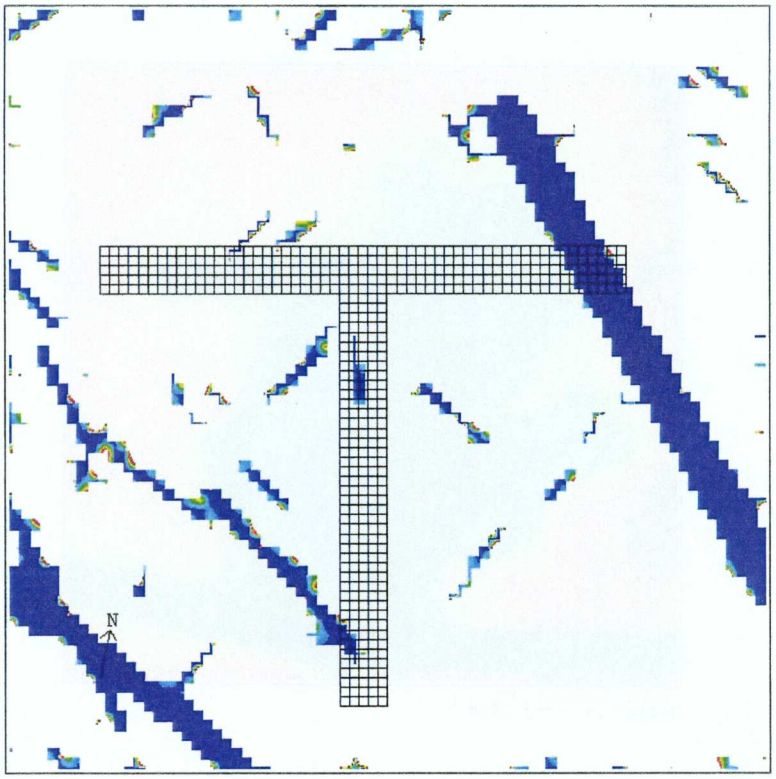

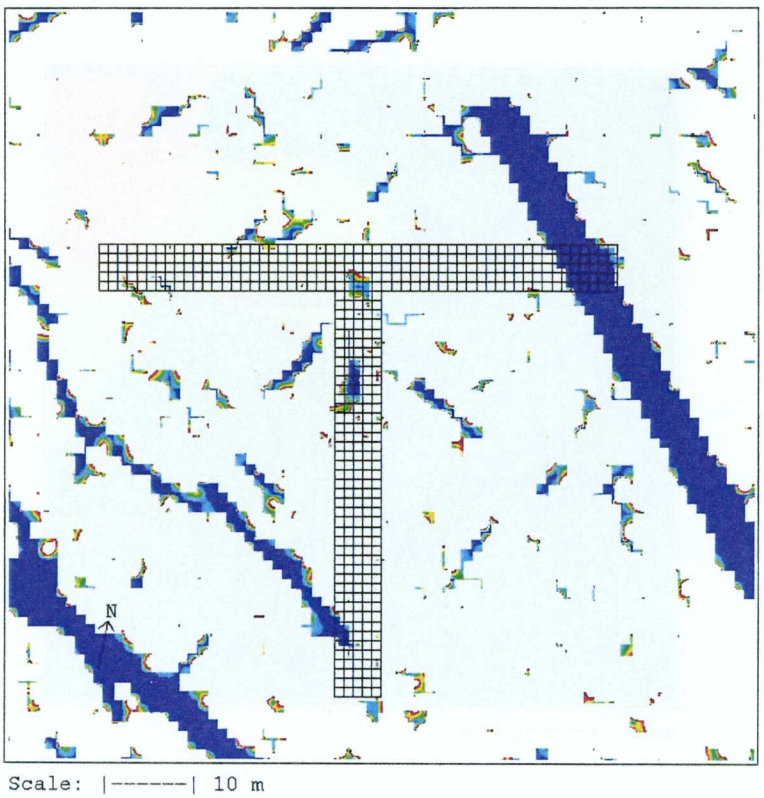

Figure 5-12. *Conductivity field for experimental volume, with isolated fractures removed (top) and with all fractures kept. Red areas have a conductivity in the range* 10^{-10} to 10^{-9} *m/s, while blue areas have a conductivity* $>10^{-9}$ *m/s.*

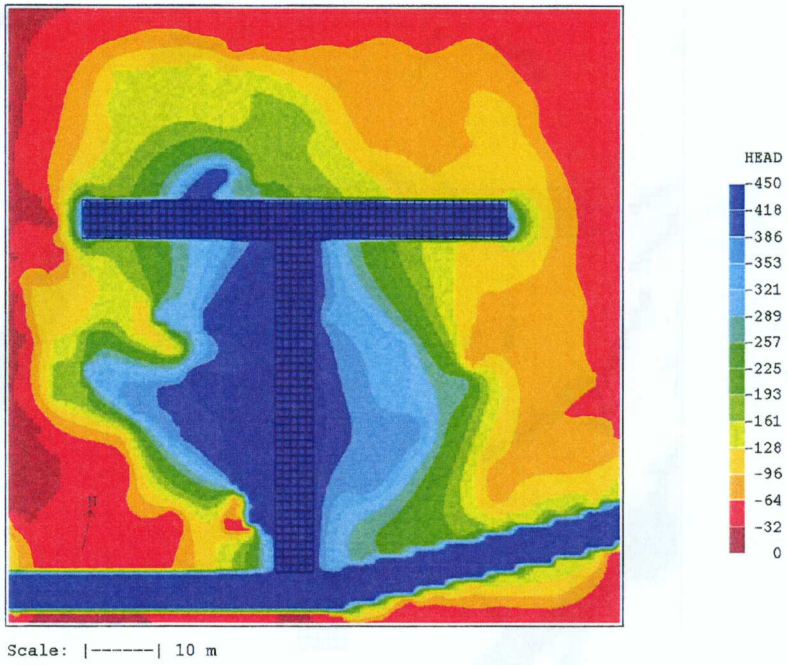

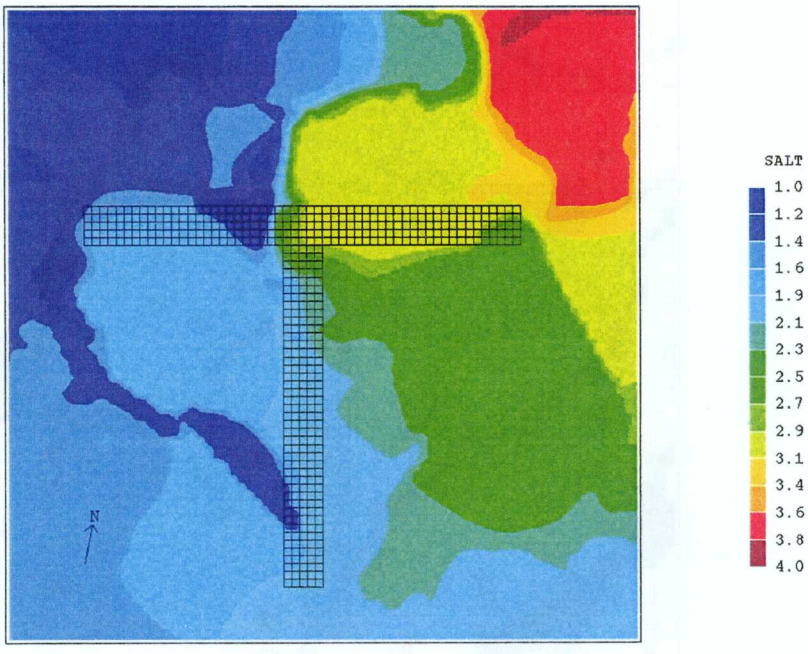

Figure 5-13. *Hydraulic head (top) and salinity (in %) distributions in the experimental volume at 450 metres depth.*

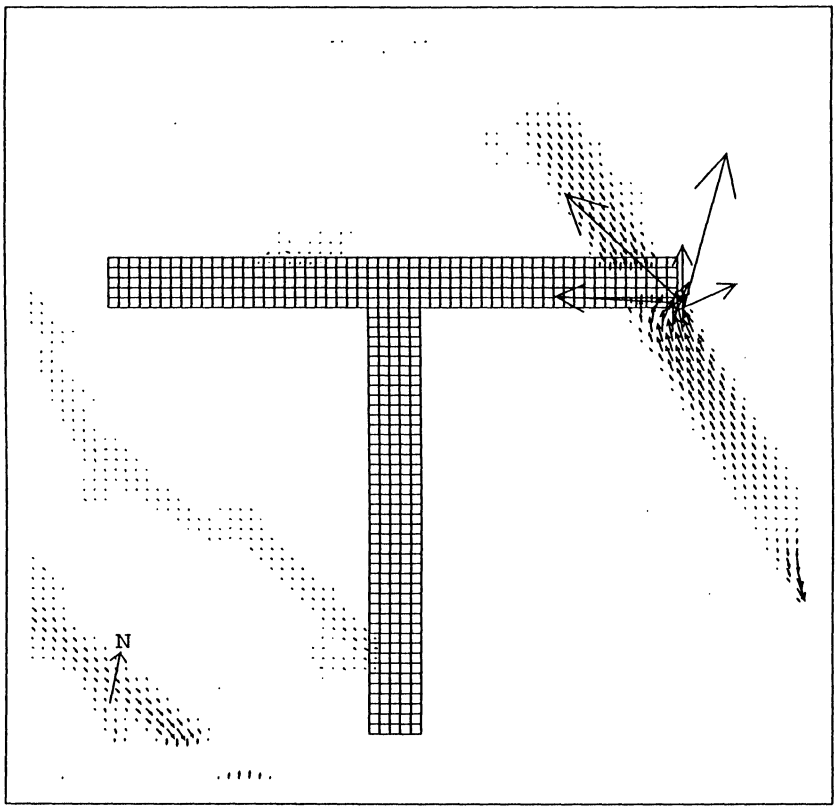

Figure 5-14. *Horizontal flow distribution in the experimental volume at a depth of 450 metres.*
Darcy velocity scale: $\longrightarrow$ 5×10^{-5} *m/s.*

6 SENSITIVITY TESTS

6.1 INTRODUCTION

The main novel feature of this study is the way the conductivity field is generated. We will therefore focus on the influence of some of the assumptions introduced in the specification of the conductivity field. The topics chosen for the sensitivity study are:

- The base realisation for the background fracture network. Two base realisations were discussed in the calibration section; here three more will be generated and drawdowns in borehole sections calculated.

- The added lognormally distributed background conductivity. In the calibration section it was argued that this added conductivity has little influence on the flow and pressure distributions. This will now be tested.

- The cut-off length in the background fracture distribution. A minimum fracture length of 5 metres was used in the laboratory model. Tests will be performed to see the influence of a larger cut-off length.

The pressure drop in borehole sections for tunnelfront position 2 875 metres will be used to demonstrate the influence of various assumptions.

6.2 RESULTS

The calculated drawdown for five different base realisations and with local realisation around boreholes can be studied in Table 6-1. It is found that the calculated drawdown may vary with about 1 metre between different realisations. The mean errors and the goodness of fit values are lower than without local realisations, see Table 4-1. It is thus concluded that the use of local realisations of the background fracture network improves the comparison with measured values and makes the conductivity field less sensitive to various realisations.

Table 6-2 shows the effect of excluding small scale features in the conductivity field. The lognormally distributed cell conductivity is found to have a very small influence on the calculated drawdowns. For all simulations shown in Table 6-2, base realisation four is used

and the case with $l_{min} = 5$ metres is thus the reference case that resulted from the calibration. It is further found that excluding fractures smaller than 40 metres does not strongly affect the calculated drawdowns. However, if fractures in the length interval 40 to 80 metres are excluded a significant influence can be detected, see for example KAS07-J3.

The conclusion from this sensitivity study is that calculated drawdowns are not very sensitive to various base realisations of the conductivity field, nor the small scale features of the conductivity field.

Table 6-1. Calculated drawdowns in borehole sections for five base realisations.

Borehole section	Measured drawdown (m)	Calculated drawdown (m) for various base realisations				
		1	2	3	4	5
K02-B4	51.50	41.39	41.43	43.10	42.12	41.52
K02-B3	16.90	26.07	26.06	26.14	26.16	26.04
K05-E4	40.40	44.09	42.41	43.20	42.39	42.90
K05-E3	30.90	39.34	40.33	41.49	40.31	40.84
K05-E2	32.50	29.60	29.57	29.24	29.06	28.93
K05-E1	29.20	27.62	27.48	27.13	27.00	27.07
K06-F4	33.80	32.69	32.30	33.58	33.02	33.37
K06-F3	13.90	28.47	30.60	30.68	29.89	29.58
K06-F2	29.10	26.28	29.13	28.82	27.69	27.41
K06-F1	30.00	25.70	28.40	27.64	26.65	26.17
K07-J4	37.50	38.18	39.11	38.38	38.59	38.61
K07-J3	25.20	25.85	30.39	26.87	26.03	26.03
K07-J2	11.70	15.63	15.74	15.63	15.51	15.54
K08-M2	16.60	24.04	22.45	22.95	23.40	22.74
K08-M1	19.50	14.10	13.93	13.99	14.05	13.94
K12-DC	25.40	28.92	28.77	29.05	28.87	29.10
K12-DB	25.30	27.91	27.61	28.64	27.60	28.45
K12-DA	24.90	28.00	27.97	29.20	27.75	28.50
K16-3	28.00	22.03	22.25	22.11	22.23	21.57
K16-2	18.60	12.21	12.23	12.20	12.19	12.23
K16-1	16.70	11.11	11.68	11.57	11.42	11.66
	Mean error	0.12	0.63	0.71	0.25	0.27
	Goodness of fit	5.86	5.97	5.88	5.84	5.91

Table 6-2. Calculated drawdowns in borehole sections without added cell-conductivity and for various values on the smallest generated fracture size, l_{min}.

Borehole section	Measured drawdown (m)	Calculated drawdown (m)					
		No background conductivity added	Smallest generated fracture, l_{min}				
			5	10	20	40	80
K02-B4	51.50	42.23	42.12	41.57	42.17	42.39	42.36
K02-B3	16.90	26.17	26.16	26.06	26.07	26.09	26.13
K05-E4	40.40	42.29	42.39	42.80	42.56	45.86	45.78
K05-E3	30.90	40.63	40.31	40.79	41.01	41.32	41.43
K05-E2	32.50	29.16	29.06	29.15	29.24	29.45	29.60
K05-E1	29.20	27.10	27.00	27.27	27.32	27.46	27.57
K06-F4	33.80	33.36	33.02	33.26	33.19	33.23	33.11
K06-F3	13.90	29.42	29.89	29.40	31.46	31.75	31.86
K06-F2	29.10	27.69	27.69	27.52	27.64	28.45	28.72
K06-F1	30.00	26.70	26.65	26.30	26.31	26.82	27.06
K07-J4	37.50	38.61	38.59	38.81	38.78	37.53	36.05
K07-J3	25.20	26.64	26.03	25.76	26.35	25.62	21.56
K07-J2	11.70	15.59	15.51	15.64	15.63	15.77	15.79
K08-M2	16.60	23.36	23.40	22.68	22.38	21.89	21.29
K08-M1	19.50	14.05	14.05	13.95	13.94	13.93	13.92
K12-DC	25.40	28.92	28.87	29.35	28.91	28.86	29.10
K12-DB	25.30	27.63	27.60	28.53	28.60	28.82	29.07
K12-DA	24.90	27.82	27.75	28.63	28.71	28.95	29.29
K16-3	28.00	22.28	22.23	21.68	21.82	21.99	22.31
K16-2	18.60	12.20	12.19	12.23	12.23	12.21	12.17
K16-1	16.70	11.46	11.42	11.89	10.96	11.20	11.11
	Mean error	0.32	0.25	0.32	0.41	0.62	0.41
	Goodness of fit	5.77	5.84	5.86	6.10	6.15	6.23

7 DISCUSSION

The present modelling study can be viewed and discussed from different aspects. It is the third step in a series of model studies, i.e. "regional", "site" and "laboratory" model. One topic for discussion centres around how the models are linked to each other (boundary conditions, equivalent conductivities for model domains, etc). However, this discussion should perhaps await the evaluation of the present laboratory model. In order to stimulate the discussion/evaluation of the laboratory model we will choose to bring up the novel features of this model for discussion.

- Background fracture network. In the laboratory model about 110 000 fracture zones and fractures are generated to form a fracture network. This network is then represented as cell conductivities in a finite-volume grid. In the author's view the method has great potential to generate conductivity fields with desired anisotropy and correlation structure. It does however require a significant amount of input data. In this study the transmissivities for the background fractures were obtained from a calibration study. In order to improve the generated conductivity fields it is thus essential to compile all relevant information (field data, theoretical arguments, structure-geological aspects, etc) and base the fracture network generation on this.

- Method of local realisation. In the calibration process it was found advantageous to optimise the fracture network by using the locally best realisation (see calibration section). It seems that this technique has two valuable properties; it can be used to improve the agreement with field data (as was done in the present calibration) and, secondly, it makes the resulting conductivity field "more deterministic", as we always keep the same realisation in the selected volumes around boreholes. The stochastic variation is due to which base realisation is used. The advantage of a "more deterministic" model is of course governed by practical considerations. An aspect of the technique that has not been discussed or evaluated so far is if the local realisations change the statistical properties of the resulting conductivity field. This needs to be evaluated.

- Local refinement. An illustration of a local refinement around an experimental volume has been described. It was assumed that the background fracture network in the laboratory model formed the deterministic fractures in the experimental volume. Fractures in the interval 0.6 to 5.0 metres were then generated,

forming the stochastic part of the fracture network. This is one way of generating the conductivity field for an experimental volume. However, the simulation raises a number of questions, see Section 5.3, concerning the fracture network for the experimental volume.

8 CONCLUDING REMARKS

A numerical model of the Äspö HRL has been developed, calibrated, applied and discussed. The model covers a volume of 800 x 600 x 360 m^3 centred around the Äspö HRL. The gridspacing is 5 metres which results in a grid with 1 382 400 cells. Boundary conditions are derived from a site scale model.

The present laboratory model is the third step in a series of model studies that started with a regional model study followed by a site scale analysis of the Äspö area. The horizontal extension of the regional model is 10 km and the resolution in the local refinement in the laboratory model is 1 metre. Except for the experimental volume, all models have been calibrated independently and boundary conditions derived from the next larger model. The three models thus constitute a systematic model study covering scales from 1 to 10 000 metres.

The novel features of the laboratory model are all related to the generation of the hydraulic conductivity field. In addition to the major (named) fracture zones a stochastically generated background fracture network is used. The method is promising as an anisotropic conductivity field with a correlation structure is generated.

The general conclusion of the study is that the model developed can simulate the conditions at the Äspö HRL in a realistic manner.

9 ACKNOWLEDGEMENT

The software package for generating the fracture network and the conductivity fields was written by Hans-Olof Kuylenstierna. His contribution has thus been of crucial importance to the project.

10 REFERENCES

Bear J, Verruijt A, 1987. Modelling Groundwater Flow and Pollution. D. Reidel Publishing Company, Dordrecht, Holland.

Follin S, Hermansson J. 1996. A discrete fracture network model of the Äspö TBM tunnel rock mass. SKB Arbets Rapport AR D-97-001.

Follin S, Hermansson J, Stigsson M, Wei L. 1998. Äspö Hard Rock Laboratory. TRUE block scale experiment. Parameters for discrete fracture network modelling - summary of initial estimations and preliminary hydraulic observations. SKB Technical Note TN-98-31b.

Hermansson J, Follin S, Wei L. 1998. Äspö Hard Rock Laboratory. TRUE block scale experiment. Input data for discrete feature network modelling of the true block scale site. Part 1 - Structural analysis of fracture traces in boreholes KA2563A and KA3510A and in the TBM tunnel. SKB Technical Note TN-97-31b.

Hermansson J, Stigsson M, Wei L. 1998. Äspö Hard Rock Laboratory. A discrete fracture network model of the Äspö ZEDEX tunnel section. SKB Progress Rapport HRL-98-29.

La Pointe P R, Wallman P, Follin S. 1995. Estimation of effective block conductivities based on discrete network analyses using data from the Äspö site. SKB Technical Report TR-95-15.

La Pointe P R, Cladouhos T, Follin S. 1999. Calculation of displacements on fractures intersecting canisters by earthquakes: Aberg, Beberg and Cberg examples. SKB Technical Report TR-99-03.

de Marsily G. and Renard Ph. 1997. Calculating equivalent permeability: a review.Advances in Water Resources. Vol. 20, Nos 5-6, pp. 253-278.

Painter S. 1999. Long-range spatial dependence in fractured rock. Empirical evidence and implications for tracer transport. SKB R-99-03.

Rhén I (ed), Gustafson G, Stanfors R, Wikberg P. 1997. Äspö HRL – Geoscientific evaluation 1997/5. Models based on site characterization 1986-1995. SKB Technical Report TR-97-06.

Rhén I, and Forsmark T, 1998. SKB Äspö Hard Rock Laboratory High-Permeability Features (HPF). Draft report.

Spalding D.B, 1981. "A general purpose computer program for multi-dimensional one- and two-phase flow". Math. Comp. Sim., 8, 267-276. See also: http://www.cham.co.uk.

Svensson U, 1997a. A regional analysis of groundwater flow and salinity distribution in the Äspö area. SKB Technical Report TR-97-09.

Svensson U, 1997b. A site scale analysis of groundwater flow and salinity distribution in the Äspö area. SKB Technical Report TR-97-17.

Svensson U, 1999. Representation of fracture networks as gridcell conductivities. SKB Technical Report TR-99-25.

APPENDIX A

DOCUMENTATION

SKB-ÄSPÖ HARD ROCK LABORATORY

Documentation of numerical simulation by Urban Svensson (US) 1999-05-26

OBJECT

SKB purchase order no:52600 98 261 2220
Title of SKB purchase order: Äspölaboratoriet – Vidareutveckling grundvattemodell, laboratoriemodell, för Äspö
Author of report: US Company: CFE AB
Operator of computer and software: US Company: CFE AB

COMPUTER

Name and version: Silicon Graphics, O2/R10 000.

SOFTWARE

Operative system: IRIX 6.3
Code name: PHOENICS 2.2 Main manual: On line
Program language: FORTRAN
Compiler: F77 for IRIX 6.3
Postprocessor name: EXPLORER Manual:
Postprocessor name: PHOTON Manual:
Subroutine: Report:
Subroutine: Report:
Subroutine: Report:

CODE VERIFICATION

Distributor: Not compiled in a single report.
Report/article:
Report/article:
Other verification
Report/article: See Svensson (1997a, 1997b and 1999), as referenced in this report.
Report/article:

INPUT DATA

Ref: Rhén et al (1997), see reference list.
Ref: Rhén and Forsmark (1998), see reference list.
Ref:
Ref:

Data file name:	Data of issue:	Stored at:
Data file name:	Data of issue:	Stored at:
Data file name:	Data of issue:	Stored at:

RESULTS

Report/article: All given in this report.
Report/article:
Data file name: Stored at:
Data file name: Stored at:

CONDENSED DESCRIPTION OF GROUNDWATER FLOW MODEL.

A laboratory scale analysis of groundwater flow and salinity distribution in the Äspö area	
Scope Groundwater and salinity distributions on a laboratory scale	
Process description Conservation of mass, volume and momentum (Darcy's law)	
CONCEPTS	**DATA**
Geometric framework and parameters	
Domain divided into computational cells to which conservation laws are applied. Subdomains consists of deterministic fracture zones and rock volumes between the fracture zones.	Domain size: 800 x 600 x 360 m^3 Computational grid: 1 382 400 cells.
Material properties	
Hydraulic conductivities (K). Density varies with salinity. Transmissivity for fracture zones (T).	Data from Rhén et al. (1997) and from calibration.
Spatial assignment method	
Fractures and fracture zones are represented in the computational grid. Small background conductivity added.	Data from Rhén et al. (1997).
Boundary conditions	
Boundary conditions from a site scale model for all boundaries.	Data from site scale model, Svensson (1997b).
Numerical tool PHOENICS	
Output parameters Flux, hydraulic head and salinity	

ISSN 1404-0344
CM Gruppen AB, Bromma, 1999